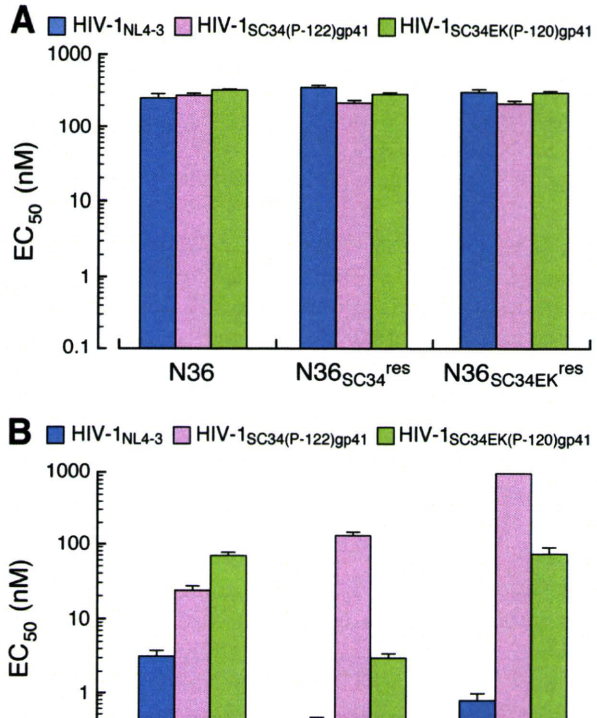

FIGURE 5. **Antiviral activity of resistant mutation-introduced peptides.** Antiviral activity of resistant mutation-introduced N36 ($N36_{SC34}^{res}$, $N36_{SC34EK}^{res}$, and original N36) (*A*) or C34 ($C34_{SC34}^{res}$, $C34_{SC34EK}^{res}$, and original C34) peptides (*B*) against HIV-1_{NL4-3} (*blue*), HIV-$1_{SC34(P-122)gp41}$ (*pink*), and HIV-$1_{SC34EK(P-120)gp41}$ (*green*) was determined using the MAGI assay. Peptide sequences are shown in Fig. 4*A*. HIV-1_{NL4-3} was used as the wild-type virus. HIV-$1_{SC34(P-122)gp41}$ contained D36G/I37K/R46K/Q52R/Q56R/N126K/S138A/E151K/K154N/N163D/L204I/L210F mutations. HIV-$1_{SC34EK(P-120)gp41}$ had D36G/Q41R/N43K/A96D/N126K/H132Y/V182I/P203S/L204I/S241F/H258Q/A312T mutations. Data are shown as mean EC_{50} values with *error bars* indicating standard deviations, obtained from at least three independent experiments.

ity and result in thermal instability of the 6-helix bundle by destabilizing the N-HR·C-HR complex. In contrast, mutations in C-HR simply enhanced the binding affinity to both wild-type and mutated N-HR.

Inhibitory Activity of Modified Fusion Inhibitors—We have previously demonstrated that introduction of resistance mutations to T-20 restores anti-HIV-1 activity against T-20-resistant variants (18), suggesting that this strategy can result in the design of peptides with improved potential for the treatment of resistant HIV-1. We examined whether this strategy was also applicable to SC34- and SC34EK-selected mutations. Hence, we introduced SC34- and SC34EK-resistant mutations that emerged in N-HR or C-HR, into the parental N36 or C34 peptides, respectively (Fig. 4*A*). Anti-HIV activities of both $N36_{SC34}^{res}$ and $N36_{SC34EK}^{res}$ showed little change compared with N36 (Fig. 5*A*), consistent with the CD analyses shown in Fig. 4, *B* and *C*, whereas mutations introduced into C34 restored their activity (Fig. 5*B*). $C34_{SC34}^{res}$ showed potent activity against HIV-1_{NL4-3} and surprisingly, it also exhibited enhanced activity against HIV-$1_{SC34EK(P-120)gp41}$. $C34_{SC34EK}^{res}$ moderately suppressed HIV-$1_{SC34EK(P-120)gp41}$, but was more effective in suppressing HIV-1_{NL4-3}, as compared with C34.

TABLE 3

Antiviral activity of fusion inhibitors to SC34- and SC34EK-selected mutation introduced HIV-1 gp41 recombinant viruses

Anti-HIV activity was determined using MAGI assay. Data are shown as mean ± S.D. obtained from at least three independent experiments, and resistance (*n*-fold of EC_{50}) of recombinant viruses, compared to that of parental HIV-1_{NL4-3}, is shown in parentheses.

Inhibitors	EC_{50} (nM)		
	HIV-1_{NL4-3} [a]	HIV-$1_{SC34(P-122)gp41}$ [b]	HIV-$1_{SC34EK(P-120)gp41}$ [c]
T-1249	0.4 ± 0.07	0.5 ± 0.06 (1.3)	0.5 ± 0.03 (1.3)
T-2410	1.0 ± 0.3	38 ± 13 (38)	3.7 ± 0.6 (3.7)
T-2429	2.2 ± 0.8	5.9 ± 1.3 (2.7)	5.4 ± 1.1 (2.5)
T-2544	0.9 ± 0.3	1.5 ± 0.5 (1.7)	1.4 ± 0.5 (1.6)
T-2635	0.3 ± 0.08	0.4 ± 0.1 (1.3)	1.1 ± 0.2 (3.7)
T-290676	0.7 ± 0.2	2.9 ± 0.8 (4.1)	4.6 ± 0.6 (6.6)
Sifuvirtide	1.7 ± 0.5	340 ± 55 (200)	35 ± 8.3 (21)
T-20EK	6.4 ± 0.8	1,548 ± 90 (242)	2,650 ± 261 (414)

[a] HIV-1_{NL4-3} was used as wild-type virus.
[b] HIV-$1_{SC34(P-122)gp41}$ has D36G/I37K/R46K/Q52R/Q56R/N126K/S138A/E151K/K154N/N163D/L204I/L210F mutations.
[c] HIV-$1_{SC34EK(P-120)gp41}$ has D36G/Q41R/N43K/A96D/N126K/H132Y/V182I/P203S/L204I/S241F/H258Q/A312T mutations.

These results further validate our strategy to overcome resistance to peptide fusion inhibitors by incorporating resistance mutations into the sequence of the original peptide inhibitor. Hence, we have been able to design peptides that can overcome resistance to T-20, C34, and now SC34 and SC34EK.

Inhibition of Resistant HIV-1 by Peptide Fusion Inhibitors—Recently, several novel peptides, including SC34 and SC34EK, have been developed as the next generation fusion inhibitors. To compare their antiviral properties, we evaluated their activities against SC34- and SC34EK-resistant HIV-1. All tested peptide fusion inhibitors showed remarkable anti-HIV-1 activity against HIV-1_{NL4-3} with EC_{50} values in the subnanomolar to nanomolar range (Table 3). However, the inhibitors had different effects on SC34- and SC34EK-resistant variants. T-1249, T-2429, T-2544, T-2635, and T-290676 retained activity against HIV-$1_{SC34(P-122)gp41}$, whereas T-2410, sifuvirtide, and T-20EK showed a decreased effect to various extents. Similarly, sifuvirtide and T-20EK had reduced activity against HIV-$1_{SC34EK(P-120)gp41}$. These results indicate that only minimal cross-resistance to the next generation of fusion inhibitors might emerge, and suggest possible successful combinations of fusion inhibitors.

DISCUSSION

To date, it remains unclear how the electrostatic constraints that are imposed on a peptide by the incorporation of EK motifs also affect the resistance profile and other virological features of these peptide fusion inhibitors. In this study, we selected HIV variants to the SC34 and SC34EK peptide inhibitors that have EK motifs, and compared their resistance profiles by comprehensive mutational analysis. SC34 and SC34EK selected several mutations within the gp41- and gp120-coding sequences over a period greater than 1 year. Phenotypic and replication kinetics analyses revealed that in the case of both inhibitors, changes in gp41 sequences served as primary mutations that decreased resistance to the inhibitors, whereas the changes in gp120 were secondary mutations compensatory in nature. However, the mutated regions of gp41 of the selected SC34- and SC34EK-resistant viruses were considerably different; mutations selected by SC34 were

mostly located within N-HR and C-HR, whereas more than half of those by SC34EK were located in another region of gp41. The molecular mechanisms and interactions that determine the effects of gp41 mutations outside the HRs on HIV-1 replication kinetics and the fusion process are not well understood. Therefore, further biological and structural studies focused on such interactions may reveal novel insights into the mechanism of fusion and the inhibition by drugs that target HIV-1 fusion.

SC34EK was designed to possess unidirectionally aligned EK pairs by modifying SC34 to have the two reverse-oriented EK pairs (Fig. 1). Thus, the difference in peptide sequences induced a different resistance pattern and reduced cross-resistance. Although accumulation of multiple mutations in gp41 eventually conferred a high level of resistance to SC34 and SC34EK, susceptibility to both inhibitors was not significantly affected by single amino acid substitutions. Moreover, it has been reported that substitutions in gp120 modulate the susceptibility to T-20 (33–36), and we also observed that both SC34- and SC34EK-selected mutations in the gp120 conferred resistance to T-20 but not to SC34 and SC34EK. These results indicate that SC34 and SC34EK have a high genetic barrier of resistance.

One mutation appeared to contribute significantly to the reduced cross-resistance of SC34- and SC34EK-resistant variants. Specifically, SC34EK selected the N43K mutation, whereas T-20 selected for N43D (31, 37), which is frequently observed together with E137K, a compensatory mutation in C-HR that maintains interaction with the N43D-substituted N-HR, possibly through the Asp^{43}-Lys^{137} ion pair (38, 39). SC34EK has been designed to harbor Lys^{137} in its peptide sequence. Hence, it is possible that resistance to SC34EK emerges through unfavorable repulsive charge-charge interactions between the Lys^{43} of the viral N-HR and the Lys^{137} residue of SC34EK. Therefore, charge interactions between amino acids 43 and 137 are likely to be the mechanism for resistance to T-20 and in part to SC34EK, but not to SC34, which has a glutamic acid (Glu^{43}) at this position. This might be one of the reasons why SC34 and SC34EK did not show significant cross-resistance.

We recently demonstrated that $T\text{-}20_{S138A}$ and $C34_{N126K}$ are able to suppress T-20- and C34-resistant variants, respectively (18). We again applied the same strategy and introduced resistance mutations in SC34 and SC34EK and examined the effect of these changes on their potency against SC34- or SC34EK-resistant variants. In this case, only mutations in the C-HR conferred enhanced susceptibility by augmenting binding affinity to the target N-HR. In the case of the $C34_{SC34EK}{}^{res}$ peptide, although we expected minimal impact of H132Y on drug susceptibility and/or on C-HR conformation, S138A appeared to stabilize the 6-helix complex by improving hydrophobic contacts with the pocket formed by Leu^{44} and Leu^{45}, as reported previously (18). In the case of the $C34_{SC34}{}^{res}$ peptide, in addition to the aforementioned S138A effect, it was expected that N126K would enable the formation of possible intra-helical salt bridges with Glu^{123} that would stabilize the α-helicity of C-HR. These mutations improved the anti-HIV-1 activity toward wild-type, and surprisingly, to SC34EK-resistant variants as well.

A number of potent peptide fusion inhibitors that suppress T-20-resistant variants have been previously reported (13, 14, 40, 41). Resistance profiles of these next generation fusion inhibitors with physicochemical modifications are expected to be different from those of the native sequence peptide fusion inhibitors, although only those of T-1249 and T-2635 were examined (42, 43). T-1249, one of the first next generation fusion inhibitors, showed potent anti-HIV-1 activity in HIV-1-infected patients that failed to respond to T-20 treatment (12). However, mutations at positions 36–45 (such as V38A/E, Q40H/K, and N43D/K), which are also observed in T-20-resistant variants *in vitro* and *in vivo*, were also detected in clinical trials of T-1249 (12, 44, 45). Nearly all the individual selected mutations had little impact on the susceptibility to T-1249. However, V38D/E conferred high-level resistance to T-1249 (30-fold) and T-20 (more than 200-fold), but not to another fusion inhibitor, T-2635 (42, 43), suggesting that there is potential cross-resistance between T-20 and T-1249. In contrast, T-2635 was hardly affected by such single mutations except for Q79E and K90E with a mild resistance of 4- and 7-fold, respectively (42), indicating that T-2635 had a preferential resistance pattern similar to SC34 and SC34EK, because these inhibitors were essentially effective against all variants with single mutations. Interestingly, although HIV-$1_{SC34(P\text{-}122)}$ and HIV-$1_{SC34EK(P\text{-}120)}$ showed mild (7.3-fold) and moderate resistance (21-fold) to C34, respectively, we observed significant differences in resistance against T-2410, another next generation fusion inhibitor, which differed from C34 by only two added amino acids at each of the N and C termini (13). Specifically, the susceptibilities of HIV-$1_{SC34(P\text{-}122)gp41}$ and HIV-$1_{SC34EK(P\text{-}120)gp41}$ to T-2410 were decreased by 38- and 3.7-fold, respectively. Although the mechanism underlying the ineffectiveness of T-2410 against SC34-resistant HIV-1 remains unclear, it appears that the size of the peptide inhibitor may be another parameter that should be considered in future attempts to design fusion peptide inhibitors with improved resistance profiles. Meanwhile, sifuvirtide and T-20EK did not show anti-HIV-1 activity against either SC34- or SC34EK-resistant variants, suggesting that they may partially share a common resistance profile. Sifuvirtide was designed based on the sequence of the C34 region of gp41 derived from HIV-1 subtype E. Similar to SC34 and SC34EK, sifuvirtide includes amino acid substitutions that could form intramolecular salt bridges. However, the majority of amino acids in sifuvirtide must be bound to the same region of N-HR, where C34, SC34, and SC34EK may interact (14). This may explain why sifuvirtide was inactive against SC34- and SC34EK-resistant variants. T-20 derivatives, including T-20EK, lack the N-terminal tryptophan-rich domain (N-TRD), also known as the pocket-binding domain, that interacts with the hydrophobic groove of the N-HR trimer (46), but they have the C-terminal TRD that interacts with the lipid bilayer at the cellular membrane (47). Our results showed that T-20-derived peptides seem less active compared with C34 derivatives with N-TRD. Recently, treatment with two or three fusion inhibitors was reported to have a potent and syn-

ergistic antiviral activity on T-20-resistant variants (48, 49). Together, these observations indicated that each inhibitor has a distinct inhibitory mechanism that may lead to the design of a combination therapy of fusion inhibitors *in vivo*.

In conclusion, the barrier for resistance to SC34 and SC34EK is considerably higher than that for the parent compound C34, or for T-20. Moreover, these inhibitors have a distinct resistance profile from C34, T-20, and other next generation fusion inhibitors. Hence, they are excellent alternatives for clinical use. Although mutations induced by SC34 and SC34EK are partially overlapped, most mutations were specific to each agent. Importantly, we demonstrated that interchange of only two pairs of EK positions could reduce cross-resistance. Because sites and direction of the EK modification seem to be easily replaceable, this is a useful strategy to suppress more efficiently emergence of resistant variants. Moreover, the present study demonstrates that the usefulness of this strategy that we have previously applied to design improved fusion inhibitors with HIV-1 sequences (18) has been extended to improve fusion inhibitors with "artificial" (non-HIV) sequences.

REFERENCES

1. Gallo, S. A., Finnegan, C. M., Viard, M., Raviv, Y., Dimitrov, A., Rawat, S. S., Puri, A., Durell, S., and Blumenthal, R. (2003) *Biochim. Biophys. Acta* **1614,** 36–50
2. Berger, E. A., Murphy, P. M., and Farber, J. M. (1999) *Annu. Rev. Immunol.* **17,** 657–700
3. Epand, R. M. (2003) *Biochim. Biophys. Acta* **1614,** 116–121
4. Chan, D. C., Fass, D., Berger, J. M., and Kim, P. S. (1997) *Cell* **89,** 263–273
5. Ryser, H. J., and Flückiger, R. (2005) *Drug Discov. Today* **10,** 1085–1094
6. O'Shea, E. K., Rutkowski, R., and Kim, P. S. (1989) *Science* **243,** 538–542
7. Wild, C., Oas, T., McDanal, C., Bolognesi, D., and Matthews, T. (1992) *Proc. Natl. Acad. Sci. U.S.A.* **89,** 10537–10541
8. Lalezari, J. P., Henry, K., O'Hearn, M., Montaner, J. S., Piliero, P. J., Trottier, B., Walmsley, S., Cohen, C., Kuritzkes, D. R., Eron, J. J., Jr., Chung, J., DeMasi, R., Donatacci, L., Drobnes, C., Delehanty, J., and Salgo, M. (2003) *N. Engl. J. Med.* **348,** 2175–2185
9. Lazzarin, A., Clotet, B., Cooper, D., Reynes, J., Arasteh, K., Nelson, M., Katlama, C., Stellbrink, H. J., Delfraissy, J. F., Lange, J., Huson, L., DeMasi, R., Wat, C., Delehanty, J., Drobnes, C., and Salgo, M. (2003) *N. Engl. J. Med.* **348,** 2186–2195
10. Mink, M., Mosier, S. M., Janumpalli, S., Davison, D., Jin, L., Melby, T., Sista, P., Erickson, J., Lambert, D., Stanfield-Oakley, S. A., Salgo, M., Cammack, N., Matthews, T., and Greenberg, M. L. (2005) *J. Virol.* **79,** 12447–12454
11. Xu, L., Pozniak, A., Wildfire, A., Stanfield-Oakley, S. A., Mosier, S. M., Ratcliffe, D., Workman, J., Joall, A., Myers, R., Smit, E., Cane, P. A., Greenberg, M. L., and Pillay, D. (2005) *Antimicrob. Agents Chemother.* **49,** 1113–1119
12. Lalezari, J. P., Bellos, N. C., Sathasivam, K., Richmond, G. J., Cohen, C. J., Myers, R. A., Jr., Henry, D. H., Raskino, C., Melby, T., Murchison, H., Zhang, Y., Spence, R., Greenberg, M. L., Demasi, R. A., and Miralles, G. D. (2005) *J. Infect. Dis.* **191,** 1155–1163
13. Dwyer, J. J., Wilson, K. L., Davison, D. K., Freel, S. A., Seedorff, J. E., Wring, S. A., Tvermoes, N. A., Matthews, T. J., Greenberg, M. L., and Delmedico, M. K. (2007) *Proc. Natl. Acad. Sci. U.S.A.* **104,** 12772–12777
14. He, Y., Xiao, Y., Song, H., Liang, Q., Ju, D., Chen, X., Lu, H., Jing, W., Jiang, S., and Zhang, L. (2008) *J. Biol. Chem.* **283,** 11126–11134
15. Nishikawa, H., Nakamura, S., Kodama, E., Ito, S., Kajiwara, K., Izumi, K., Sakagami, Y., Oishi, S., Ohkubo, T., Kobayashi, Y., Otaka, A., Fujii, N., and Matsuoka, M. (2009) *Int. J. Biochem. Cell Biol.* **41,** 891–899
16. Marqusee, S., and Baldwin, R. L. (1987) *Proc. Natl. Acad. Sci. U.S.A.* **84,** 8898–8902
17. Otaka, A., Nakamura, M., Nameki, D., Kodama, E., Uchiyama, S., Nakamura, S., Nakano, H., Tamamura, H., Kobayashi, Y., Matsuoka, M., and Fujii, N. (2002) *Angew. Chem. Int. Ed. Engl.* **41,** 2937–2940
18. Izumi, K., Kodama, E., Shimura, K., Sakagami, Y., Watanabe, K., Ito, S., Watabe, T., Terakawa, Y., Nishikawa, H., Sarafianos, S. G., Kitaura, K., Oishi, S., Fujii, N., and Matsuoka, M. (2009) *J. Biol. Chem.* **284,** 4914–4920
19. Watabe, T., Terakawa, Y., Watanabe, K., Ohno, H., Nakano, H., Nakatsu, T., Kato, H., Izumi, K., Kodama, E., Matsuoka, M., Kitaura, K., Oishi, S., and Fujii, N. (2009) *J. Mol. Biol.* **392,** 657–665
20. Aquaro, S., D'Arrigo, R., Svicher, V., Perri, G. D., Caputo, S. L., Visco-Comandini, U., Santoro, M., Bertoli, A., Mazzotta, F., Bonora, S., Tozzi, V., Bellagamba, R., Zaccarelli, M., Narciso, P., Antinori, A., and Perno, C. F. (2006) *J. Antimicrob. Chemother.* **58,** 714–722
21. Chibo, D., Roth, N., Roulet, V., Skrabal, K., Gooey, M., Carolan, L., Nicholls, J., Papadakis, A., and Birch, C. (2007) *AIDS* **21,** 1974–1977
22. Chackerian, B., Long, E. M., Luciw, P. A., and Overbaugh, J. (1997) *J. Virol.* **71,** 3932–3939
23. Adachi, A., Gendelman, H. E., Koenig, S., Folks, T., Willey, R., Rabson, A., and Martin, M. A. (1986) *J. Virol.* **59,** 284–291
24. Nameki, D., Kodama, E., Ikeuchi, M., Mabuchi, N., Otaka, A., Tamamura, H., Ohno, M., Fujii, N., and Matsuoka, M. (2005) *J. Virol.* **79,** 764–770
25. Naito, T., Izumi, K., Kodama, E., Sakagami, Y., Kajiwara, K., Nishikawa, H., Watanabe, K., Sarafianos, S. G., Oishi, S., Fujii, N., and Matsuoka, M. (2009) *Antimicrob. Agents Chemother.* **53,** 1013–1018
26. Shimura, K., Kodama, E., Sakagami, Y., Matsuzaki, Y., Watanabe, W., Yamataka, K., Watanabe, Y., Ohata, Y., Doi, S., Sato, M., Kano, M., Ikeda, S., and Matsuoka, M. (2008) *J. Virol.* **82,** 764–774
27. Oishi, S., Ito, S., Nishikawa, H., Watanabe, K., Tanaka, M., Ohno, H., Izumi, K., Sakagami, Y., Kodama, E., Matsuoka, M., and Fujii, N. (2008) *J. Med. Chem.* **51,** 388–391
28. Kuiken, C., Leitner, T., Foley, B., Hahn, B., Marx, P., McCutchan, F., Wolinsky, S., and Korber, B. (eds) (2008) *HIV Sequence Compendium,* Los Alamos National Laboratory, Theoretical Biology and Biophysics, Los Alamos, NM
29. Rimsky, L. T., Shugars, D. C., and Matthews, T. J. (1998) *J. Virol.* **72,** 986–993
30. Lu, J., Deeks, S. G., Hoh, R., Beatty, G., Kuritzkes, B. A., Martin, J. N., and Kuritzkes, D. R. (2006) *J. Acquir. Immune Defic. Syndr.* **43,** 60–64
31. Melby, T., Sista, P., DeMasi, R., Kirkland, T., Roberts, N., Salgo, M., Heilek-Snyder, G., Cammack, N., Matthews, T. J., and Greenberg, M. L. (2006) *AIDS Res. Hum. Retroviruses* **22,** 375–385
32. Cabrera, C., Marfil, S., García, E., Martinez-Picado, J., Bonjoch, A., Bofill, M., Moreno, S., Ribera, E., Domingo, P., Clotet, B., and Ruiz, L. (2006) *AIDS* **20,** 2075–2080
33. Derdeyn, C. A., Decker, J. M., Sfakianos, J. N., Wu, X., O'Brien, W. A., Ratner, L., Kappes, J. C., Shaw, G. M., and Hunter, E. (2000) *J. Virol.* **74,** 8358–8367
34. Derdeyn, C. A., Decker, J. M., Sfakianos, J. N., Zhang, Z., O'Brien, W. A., Ratner, L., Shaw, G. M., and Hunter, E. (2001) *J. Virol.* **75,** 8605–8614
35. Reeves, J. D., Gallo, S. A., Ahmad, N., Miamidian, J. L., Harvey, P. E., Sharron, M., Pohlmann, S., Sfakianos, J. N., Derdeyn, C. A., Blumenthal, R., Hunter, E., and Doms, R. W. (2002) *Proc. Natl. Acad. Sci. U.S.A.* **99,** 16249–16254
36. Reeves, J. D., Miamidian, J. L., Biscone, M. J., Lee, F. H., Ahmad, N., Pierson, T. C., and Doms, R. W. (2004) *J. Virol.* **78,** 5476–5485
37. Sista, P. R., Melby, T., Davison, D., Jin, L., Mosier, S., Mink, M., Nelson, E. L., DeMasi, R., Cammack, N., Salgo, M. P., Matthews, T. J., and Greenberg, M. L. (2004) *AIDS* **18,** 1787–1794
38. Tolstrup, M., Selzer-Plön, J., Laursen, A. L., Bertelsen, L., Gerstoft, J., Duch, M., Pedersen, F. S., and Ostergaard, L. (2007) *AIDS* **21,** 519–521
39. Bai, X., Wilson, K. L., Seedorff, J. E., Ahrens, D., Green, J., Davison, D. K., Jin, L., Stanfield-Oakley, S. A., Mosier, S. M., Melby, T. E., Cammack, N., Wang, Z., Greenberg, M. L., and Dwyer, J. J. (2008) *Biochemistry* **47,** 6662–6670

40. He, Y., Cheng, J., Lu, H., Li, J., Hu, J., Qi, Z., Liu, Z., Jiang, S., and Dai, Q. (2008) *Proc. Natl. Acad. Sci. U.S.A.* **105,** 16332–16337
41. Qi, Z., Shi, W., Xue, N., Pan, C., Jing, W., Liu, K., and Jiang, S. (2008) *J. Biol. Chem.* **283,** 30376–30384
42. Eggink, D., Baldwin, C. E., Deng, Y., Langedijk, J. P., Lu, M., Sanders, R. W., and Berkhout, B. (2008) *J. Virol.* **82,** 6678–6688
43. Eggink, D., Langedijk, J. P., Bonvin, A. M., Deng, Y., Lu, M., Berkhout, B., and Sanders, R. W. (2009) *J. Biol. Chem.* **284,** 26941–26950
44. Melby, T., Demasi, R., Cammack, N., Miralles, G. D., and Greenberg, M. L. (2007) *AIDS Res. Hum. Retroviruses* **23,** 1366–1373
45. Eron, J. J., Gulick, R. M., Bartlett, J. A., Merigan, T., Arduino, R., Kilby, J. M., Yangco, B., Diers, A., Drobnes, C., DeMasi, R., Greenberg, M., Melby, T., Raskino, C., Rusnak, P., Zhang, Y., Spence, R., and Miralles, G. D. (2004) *J. Infect. Dis.* **189,** 1075–1083
46. Chan, D. C., Chutkowski, C. T., and Kim, P. S. (1998) *Proc. Natl. Acad. Sci. U.S.A.* **95,** 15613–15617
47. Salzwedel, K., West, J. T., and Hunter, E. (1999) *J. Virol.* **73,** 2469–2480
48. Pan, C., Cai, L., Lu, H., Qi, Z., and Jiang, S. (2009) *J. Virol.* **83,** 7862–7872
49. Pan, C., Lu, H., Qi, Z., and Jiang, S. (2009) *AIDS* **23,** 639–641

研究成果の刊行に関する一覧表

研究代表者：京都大学ウイルス研究所　松岡 雅雄
研究分担者：京都大学大学院薬学研究科　藤井 信孝
大石 真也

雑誌

発表者氏名	論文タイトル名	発表誌名	巻号	ページ	出版年
Izumi K., Nakamura S., Nakano H., Shimura K., Sakagami Y., Oishi S., Uchiyama S., Ohkubo T, Kobayashi Y., Fujii N., Matsuoka M., Kodama E.N.	Characterization of HIV-1 resistance to a fusion inhibitor, N36, derived from the gp41 amino terminal heptad repeat	Antiviral Res.	87(2)	179-186	2010
Oishi S., Watanabe K., Ito S.; Tanaka M.; Nishikawa H.; Ohno H.; Shimane K.; Izumi K.; Sakagami Y.; Kodama E. N.; Matsuoka M.; Asai A.; Fujii N.	Affinity selection and sequence-activity relationships of HIV-1 membrane fusion inhibitors directed at the drug-resistant variants.	Med. Chem. Commun.	1(4)	276-281	2010
Omatsu Y., Sugiyama T., Kohara H., Kondoh G., Fujii N., Kohno K., Nagasawa T.	The essential functions of adipoosteogenic progenitors as the hematopoietic stem and progenitor cell niche.	Immunity	33(3)	387-399	2010
Mandawat A., Fiskus W., Buckley K.M., Robbins K., Rao R., Balusu R., Navenot J.M., Wang Z.X., Ustun C., Chong D.G., Atadja P., Fujii N., Peiper S.C., Bhalla K.	Pan-histone deacetylase (HDAC) inhibitor panobinostat depletes CXCR4 levels and signaling and exerts synergistic anti-myeloid activity in combination with CXCR4 antagonists	Blood	116(24)	5306-5315	2010
Martin S.K, Diamond P., Williams S.A., To L.B., Peet D.J., Fujii N., Gronthos S., Harris A.L., Zannettino A.C.	Hypoxia-inducible factor-2 is a novel regulator of aberrant CXCL12 expression in multiple myeloma plasma cells	Haematologica	95(5)	776-784	2010

Gravel S., Malouf C., Boulais P.E., Berchiche Y.A., Oishi S., Fujii N., Leduc R., Sinnett D., Heveker N.	The peptidomimetic CXCR4 antagonist TC14012 recruits β-arrestin to CXCR7 roles of receptor domains	J. Biol. Chem.	285(49)	37939-37943	2010
Shimura K., Nameki D., Kajiwara K., Watanabe K., Sakagami Y., Oishi S., Fujii N., Matsuoka M.., Sarafianos S.G., Kodama E.	Resistance profiles of novel electrostatically constrained HIV-1 fusion inhibitors	J. Biol. Chem.	285(50)	39471-39480	2010
Noda M., Omatsu Y., Sugiyama T., Oishi S., Fujii N., Nagasawa T.	CXCL12-CXCR4 chemokine signaling is essential for NK cell development in adult mice	Blood	117(2)	451-458	2011
Inokuchi E., Yamada A., Hozumi K., Tomita K., Oishi S., Ohno H., Nomizu M., Fujii N.	Design and synthesis of amidine-type peptide bond isostere: application of nitrile oxide derivatives as active ester equivalents to peptide and peptidomimetics synthesis.	Org. Biomol. Chem.	9(9)	3421-3427	2011
Xu C, Liu J, Chen L, Liang S, Fujii N, Tamamura H, Xiong H.	HIV-1 gp120 enhances outward potassium current via CXCR4 and cAMP-dependent protein kinase a signaling in cultured rat microglia	Glia,	59(6)	997-1007	2011
Masuda R., Oishi S., Ohno H., Kimura H., Saji H., Fujii N.	Concise site-specific synthesis of DTPA-peptide conjugates: application to imaging probes f r the chemokine receptor CXCR4.	Bioorg. Med. Chem.	19(10)	3216-3220	2011
Inokuchi E., Oishi S., Kubo T., Ohno H., Shimura K., Matsuoka M., Fujii N.	Potent CXCR4 antagonists containing amidine-type peptide bond isosteres.	ACS Med. Chem. Lett.	2(1)	53-57	2011

Affinity selection and sequence-activity relationships of HIV-1 membrane fusion inhibitors directed at the drug-resistant variants†

Shinya Oishi,*[a] Kentaro Watanabe,[a] Saori Ito,[a] Michinori Tanaka,[a] Hiroki Nishikawa,[a] Hiroaki Ohno,[a] Kazuki Shimane,[b] Kazuki Izumi,[b] Yasuko Sakagami,[b] Eiichi N. Kodama,‡[b] Masao Matsuoka,[b] Akira Asai[c] and Nobutaka Fujii*[a]

Received 29th June 2010, Accepted 22nd July 2010
DOI: 10.1039/c0md00091d

Enfuvirtide is the first approved membrane fusion inhibitor against HIV-1. Although this drug is effective against multi-drug resistant strains, the emergence of enfuvirtide-resistant strains has been reported in patients who have received an enfuvirtide-containing regimen. Based on the high affinity of synthetic HIV-1 gp41 C-terminal heptad repeat (C-HR) peptides to the counterpart trimeric N-terminal heptad repeat (N-HR) coiled-coil structure, a novel screening approach has been established to facilitate the identification of potent fusion inhibitors against wild-type and enfuvirtide-resistant HIV-1. In this process, affinity selection using histidine-tagged N-HR peptides with the sequences derived from wild-type and resistant strains efficiently captured potent inhibitory peptides from a pool of highly water-soluble C-HR peptides with α-helix-inducible motifs. A highly potent peptide was found from a single amino acid substitution observed in an enfuvirtide-resistant variant as well as peptides with unprecedented modifications at the mutated site.

Introduction

Several inhibitors that block viral attachment and the fusion process have been approved for the treatment of human immunodeficiency virus (HIV) in the past decade. The first fusion inhibitor, enfuvirtide (T-20), binds to the N-terminal heptad repeat (N-HR) of the HIV-1 envelop glycoprotein gp41,[1] and prevents the formation of a fusogenic antiparallel coiled-coil structure (known as the six-helical bundle) between N-HR and the C-terminal heptad repeat (C-HR) (Fig. 1a).[2] Enfuvirtide is effective even against the clinical strains that are resistant to multiple drug classes such as reverse transcriptase inhibitors and protease inhibitors used in highly active antiretroviral therapy (HAART). However, the emergence of enfuvirtide-resistant strains has been reported in patients receiving long-term enfuvirtide treatment.[3,4]

The primary evolution of enfuvirtide resistance occurs on gp41 N-HR, which attenuates the binding affinity with enfuvirtide, resulting in decreased drug susceptibility.[3–5] The major primary mutations are V38A and N43D in the Leu33–Leu45 region of N-HR. These mutations subsequently lead to a secondary mutation appearing in C-HR, which can compensate the binding affinity between viral N-HR and C-HR for efficient gp41 folding.[6] For example, N126K and S138A mutations have been reported to enhance the resistance induced by enfuvirtide and another inhibitory C-HR peptide, C34. These complementary mutations, which occur at the face-to-face positions of N-HR and C-HR verified by crystallographic studies,[7–9] can restore the critical step required for viral infection into the target cells and eliminate the inhibitory effect of exogenous enfuvirtide.

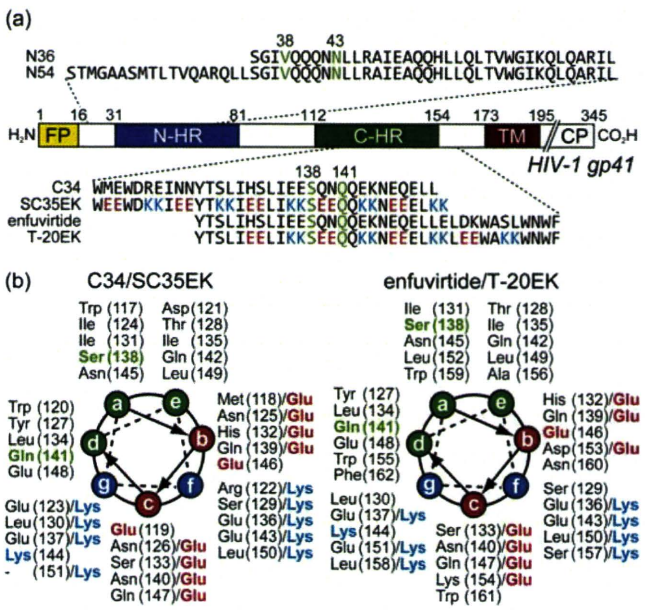

Fig. 1 HIV-1 envelope protein gp41 and the amino acid sequences. (a) Schematic representation of HIV-1 gp41. FP: fusion peptide; TM: transmembrane domain; CP: cytoplasmic tail. (b) Helical-wheel representation of C34/SC35EK and enfuvirtide/T-20EK.

[a]*Graduate School of Pharmaceutical Sciences, Kyoto University, Sakyo-ku, Kyoto 606-8501, Japan. E-mail: soishi@pharm.kyoto-u.ac.jp; nfujii@pharm.kyoto-u.ac.jp; Fax: +81-75-753-4570; Tel: +81-75-753-4551*

[b]*Laboratory of Virus Control, Institute for Virus Research, Kyoto University, Sakyo-ku, Kyoto 606-8507, Japan*

[c]*Graduate School of Pharmaceutical Sciences, University of Shizuoka, Suruga-ku, Shizuoka 422-8526, Japan*

† Electronic supplementary information (ESI) available: Additional experimental procedures, measurement of CD spectra, bioassays, and MS data. See DOI: 10.1039/c0md00091d

‡ Present address: Division of Emerging Infectious Diseases, Tohoku University School of Medicine, Sendai 980-8575, Japan

Recently, several novel fusion inhibitors such as tifuvirtide (T-1249)[10] and sifuvirtide,[11] which are effective against these enfuvirtide-resistant viruses, have been reported. We have also demonstrated a novel tailored design of fusion inhibitors based on the enfuvirtide-resistant mutation to preempt this escape strategy of HIV-1.[12] Enfuvirtide analogues carrying a substitution corresponding to the secondary mutation were found to exert potent anti-HIV activity against wild-type and enfuvirtide-resistant strains with the primary mutations. Of interest, during this observation, we found that enfuvirtide analogues with other substitutions were also effective against these strains. Alternatively, modification of a single residue in C-HR such as Q141L, which is involved in the increased syncytium-forming ability of the mutant virus,[13] led to an increase in the anti-HIV potency of inhibitor C34.[14] These observations implied that the C-HR sequence with substitutions, which were not spontaneously elaborated by single nucleotide mutations from wild-type HIV-1, could represent potent fusion inhibitors. Encouraged by these results, the optimization of interactive residues of fusion inhibitors against wild-type and enfuvirtide-resistant viruses was undertaken.

Affinity selection-mass spectrometry (AS-MS) is a promising methodology for compound screening, in which target molecule-bound components are captured from a pool of candidates and are identified by mass spectrometry. The successful applications of this technique are exemplified by the identification of kinase inhibitors[15] and antifungal natural products.[16] This simple selection process by virtue of the binding affinity can be a facile alternative to functional bioassays, although the functions and mechanisms of captured compounds for bioactivity cannot be determined. For medicinal chemistry of HIV fusion inhibitors, this approach should be suitable in the optimization of inhibitory C-HR peptides such as T-20EK[17] and SC35EK.[18] Taking advantage of the trimeric N-HR coiled-coil as a target molecule, a mixture of C-HR peptides with a single amino acid substitution can be screened without using recombinant or clinical HIV strains.[19,20] We envisioned that the competitive binding of C-HR components would capture relatively more potent anti-HIV peptides with higher affinity towards N-HR. Herein we report on the affinity-based screening technology and sequence-activity relationships for amino acid optimization in HIV-1 fusion inhibitors directed against enfuvirtide-resistant HIV strains.

Results and discussion

T-20EK and SC35EK are characterized by repeated X-EE-XX-KK motifs that stabilize the bioactive α-helix structure of enfuvirtide and C34, respectively (Fig. 1a). Potential electrostatic interactions between glutamic acid (Glu) and lysine (Lys) residues at i and $i + 4$ positions, respectively, are distinct from the traditional stabilization with stapled covalent linkages.[21,22] Consistent substitution of the residues located on the non-interactive surface of the C-HR α-helix with Glu or Lys achieved an enhancement in affinity toward the N-HR sequence and anti-HIV activity. This process disclosed the indispensable residues in C-HR for direct interaction with viral N-HR (Fig. 1b).[23] Additionally, in contrast to native sequences of C-HR peptides that are highly hydrophobic, substitution with charged amino acids markedly improved the aqueous solubility of the peptides. This design allowed us to prepare a homogeneous mixture of the SC35EK derivatives and T-20EK derivatives at high concentrations.

Initially, C-HR peptide libraries with a variety of canonical amino acid substitutions at the positions to be optimized (Ser138 and Gln141) were prepared by a split-pool method. After the construction of the C-terminal sequence using a standard Fmoc-based solid-phase peptide synthesis approach, the resin was split into fractions at position 138 or 141, where proteinogenic amino acids except for cysteine were coupled in parallel. The 19 fractions were combined again and the N-terminal sequence was constructed in one portion. All the protected peptide resins were treated with a cocktail of deprotection reagents, and the crude peptides were purified by reversed-phase HPLC to afford the expected peptides.

Separately, in order to rationalize the selection process by affinity-based technology and to investigate the sequence-activity relationship, all C-HR peptides with a single substitution were prepared in parallel and were evaluated for the biological and physicochemical properties individually. The counterpart N-HR peptides of the wild-type and enfuvirtide-resistant variants (V38A and N43D) were also prepared. For affinity selection, the histidine tag (His_6) sequence of the N-HR peptides was attached on the N-terminus *via* an aminocaproic acid-glycine dipeptide linker. This linker was incorporated to avoid the possible disruption of N-HR and C-HR interaction by positively charged His_6-tag. Anti-HIV activities of all the C-HR peptides against laboratory wild-type HIV-1_{NL4-3} or the variants with enfuvirtide-resistant mutations were evaluated using the MAGI assay. Thermal stabilities of the potential six-helical bundles consisting of N-HR and C-HR peptides were evaluated by measuring the melting temperature (T_m) using the molar ellipticity value at 222 nm in circular dichroic (CD) spectra of N36/SC35EK or N54/T-20EK mixture (Figure S1, ESI†).

The AS-MS protocol was optimized using SC35EK derivatives (Table 1). A pool of $SC35EK_{S138X}$ was incubated with a wild-type N-HR peptide, N36 (10 μM) with an N-terminal His_6-tag, in HEPES buffer (pH 7.4). The potential six-helical bundles of N36–$SC35EK_{S138X}$ were captured by Ni-NTA agarose resin and were subsequently eluted with 50% AcOH (Fig. 2a). The captured components were separated and characterized by LC-MS analysis, except that the peptides with Leu and Ile were observed as overlapping peaks of the same mass-to-charge ratio (Fig. 2b). The recovery rate in affinity selection for relative binding ability to N36 was calculated from the detected signal of $[M + 3H]^{3+}$ and $[M + 4H]^{4+}$ ions of each C-HR peptide by the LC-MS analysis of captured peptides. Under the high concentration conditions (10 μM each of $SC35EK_{S138X}$), several potent peptides including a resistant variant-derived S138A peptide were captured in high recovery rates, while slightly less potent peptides such as $SC35EK_{S138F}$ and $SC35EK_{S138Y}$ were not detected. In contrast, when the total concentration of the mixture was nearly equal to the N36 concentration (0.6 μM each of $SC35EK_{S138X}$), there was no discernible difference in the recovery rates of each peptide. The compound with the least potent anti-HIV activity in the series, $SC35EK_{S138R}$, was recovered under this equimolar concentration conditions. This recovery suggested that the method is not effective under lower concentration conditions of C-HR peptides. A condition using

Table 1 Optimization of the affinity selection protocol

	Recovery (%)[a]					
	Concentration of $SC35EK_{S138X}$/μM					
X	10	6	1	0.6	EC_{50}/nM[b]	T_m/°C[c]
Ser	22.8	19.2	11.5	5.8	1.0 ± 0.14	81.6
Ala	30.7	22.5	11.5	5.3	1.2 ± 0.12	86.4
Asp	0.7	0.0	0.0	4.3	15 ± 3.3	59.7
Glu	1.3	1.0	1.8	5.1	15 ± 0.69	66.2
Phe	0.7	0.6	4.0	6.3	1.5 ± 0.10	72.9
Gly	13.8	14.4	11.6	5.9	1.9 ± 0.26	79.1
His	0.9	0.6	2.4	5.7	1.9 ± 0.57	62.9
Ile	4.7[d]	7.6[d]	11.3[d]	6.9[d]	1.3 ± 0.54	84.6
Lys	0.2	0.1	0.0	3.6	8.2 ± 1.7	53.5
Leu	4.7[d]	7.6[d]	11.3[d]	6.9[d]	0.93 ± 0.16	83.2
Met	8.9	13.3	12.5	6.8	0.68 ± 0.06	84.1
Asn	1.1	0.5	4.3	6.4	2.2 ± 0.47	69.0
Pro	0.4	0.2	0.1	4.5	35 ± 9.2	56.1
Gln	0.9	0.5	2.1	6.1	2.4 ± 0.79	65.9
Arg	0.3	0.1	0.0	2.5	280 ± 47	52.3
Thr	9.0	12.8	11.7	5.7	1.8 ± 0.27	79.7
Val	2.8	6.0	12.1	7.0	1.9 ± 0.64	79.9
Trp	0.5	0.3	0.9	6.2	3.1 ± 0.52	66.4
Tyr	0.5	0.4	2.3	5.9	1.9 ± 0.71	68.0

[a] The recovery rate was determined from the relative detected signals of $[M + 3H]^{3+}$ and $[M + 4H]^{4+}$ ions by LC-MS analysis. [b] EC_{50} was determined as the concentration that blocked $HIV\text{-}1_{NL4\text{-}3}$ replication by 50% in the MAGI assay. To improve the replication kinetics, the D36G mutation, observed in the majority of HIV-1 strains, was introduced into the NL4-3 background used in this study. [c] T_m values were defined by the midpoint of the thermal unfolding transition state measured by monitoring the molar ellipticity at 222 nm of N36/$SC35EK_{S138X}$ mixture. [d] Combined yield of 138I and 138L derivatives.

1 μM each of $SC35EK_{S138X}$ (total 19 μM of the mixture) for affinity selection was selected for further experiments, in which the recovery rate was found to positively correlate with the stability of the six-helical bundle (Fig. 3a). Although an ideal linear correlation was not observed between the logarithmic EC_{50} of anti-HIV activity and the recovery rate (Fig. 3b), the peptides, which were captured in relatively high yields by affinity selection, exhibited highly potent anti-HIV activity.

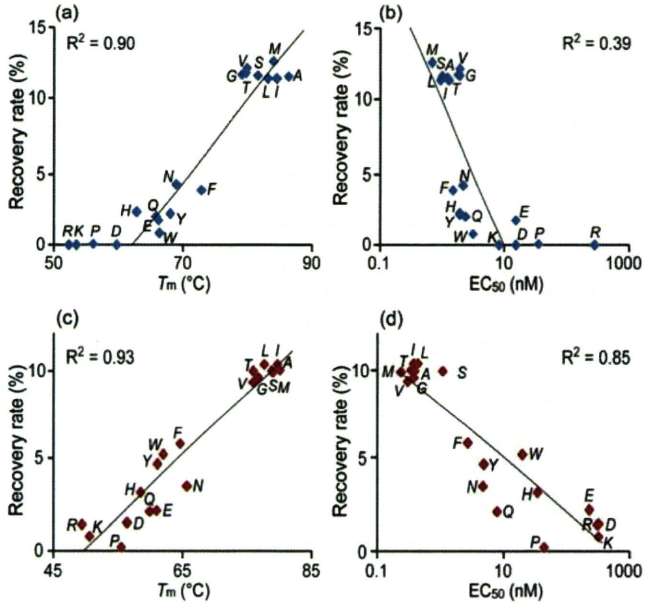

Fig. 3 Correlation between the recovery rate and the thermal stability, or the anti-HIV activity. (a, b) $SC35EK_{S138X}$; (c, d) $T\text{-}20EK_{S138X}$. R^2 values for the correlation of $SC35EK_{S138X}$ data were calculated without using the data points of S138R/K/P/D mutants ($n = 15$).

The optimized condition was applied for the selection of $T\text{-}20EK_{S138X}$ derivatives (Table 2). The anti-HIV activity of $T\text{-}20EK_{S138X}$ was found to be dependent on the amino acid type at position 138. Substitution with aliphatic side-chain amino acids such as Ala, Ile, Leu, Met and Val, displayed highly potent anti-HIV activity, although significant stabilization of the N54–$T\text{-}20EK_{S138X}$ complexes was not observed. Gly- and Thr-substitutions were also observed to increase potency. In contrast, hydrophilic, charged and aromatic amino acid substitutions at position 138 reduced binding with N54. In our previous study, it was demonstrated that higher affinity with the N-HR sequence and more potent anti-HIV activity of $C34_{S138A}$ and $T\text{-}20_{S138A}$ were due to the dominant contribution of larger desolvation free energy of the hydrophobic side-chain.[8] The structure–activity

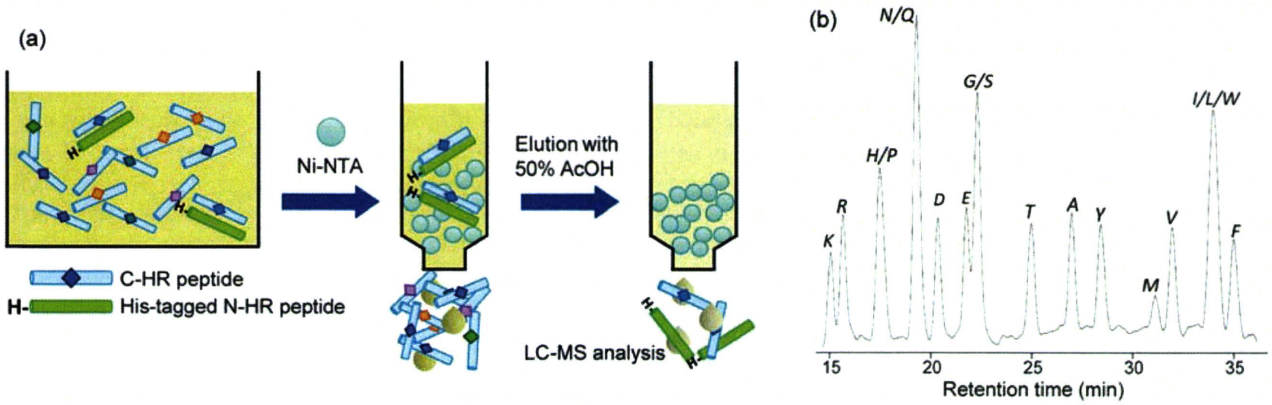

Fig. 2 Affinity selection of the HIV-1 fusion inhibitors. (a) Protocol outlining the affinity selection of C-HR peptides using the histidine-tagged N-HR peptide. (b) HPLC profile of a pool of SC35EK derivatives with a single amino acid substitution at position 138 [Cosmosil 5C18 AR-II column; linear 30–40% MeCN gradient over 40 min; flow rate, 1 cm^3 min^{-1}; detection at 220 nm].

Table 2 Recovery rate in affinity selection and anti-HIV activity of T-20EK$_{S138X}$, and the thermal stability of the N54–T-20EK$_{S138X}$ complex

X	Recovery (%)[a]	EC_{50}/nM[b]	T_m/°C[c]	X	Recovery (%)[a]	EC_{50}/nM[b]	T_m/°C[c]
Ser	10.0	1.1 ± 0.2	78.8				
Ala	10.0	0.3 ± 0.1	80.1	Met	9.9	0.2 ± 0.1	79.0
Asp	1.5	330 ± 96	56.5	Asn	3.5	4.8 ± 1.6	65.7
Glu	2.2	230 ± 31	61.0	Pro	0.2	44 ± 8	55.5
Phe	5.8	2.8 ± 0.2	64.6	Gln	2.2	7.9 ± 3.4	60.0
Gly	9.6	0.4 ± 0.2	76.7	Arg	1.5	320 ± 88	49.4
His	3.2	35 ± 10	58.5	Thr	10.0	0.4 ± 0.2	75.9
Ile	10.4[d]	0.4 ± 0.1	79.7	Val	9.4	0.3 ± 0.1	76.0
Lys	0.8	330 ± 67	50.6	Trp	5.2	20 ± 9	62.0
Leu	10.4[d]	0.4 ± 0.3	77.6	Tyr	4.7	5.0 ± 1.5	61.1

[a] The recovery rate was determined from the relative detected signals of $[M + 3H]^{3+}$ and $[M + 4H]^{4+}$ ions by LC-MS analysis. [b] EC_{50} was determined as the concentration that blocked HIV-1_{NL4-3} replication by 50% in the MAGI assay. To improve the replication kinetics, the D36G mutation, observed in the majority of HIV-1 strains, was introduced into the NL4-3 background used in this study. [c] T_m values were defined by the midpoint of the thermal unfolding transition state measured by monitoring the molar ellipticity at 222 nm of N54/T-20EK$_{S138X}$ mixture. [d] Combined yield of 138I and 138L derivatives.

Table 3 Peptide recovery in affinity selection, anti-HIV activity and thermal stability of the six-helix bundles of C-HR peptides against enfuvirtide-resistant variants

	SC35EK$_{S138X}$			T-20EK$_{S138X}$		
X	Recovery (%)[a]	EC_{50}/nM[b]	T_m/°C[c]	Recovery (%)[a]	EC_{50}/nM[b]	T_m/°C[c]
HIV$_{V38A}$						
Ser	11.8	1.1 ± 0.3	72.6	9.3	3.4 ± 1.4	60.0
Ala	11.4	0.7 ± 0.2	76.1	10.0	2.2 ± 0.8	64.6
Leu	10.3[d]	0.8 ± 0.1	75.0	10.1[d]	3.4 ± 1.6	57.5
Pro	0.4	340 ± 61	56.3	0.0	>1000	49.7
Thr	10.8	0.8 ± 0.1	70.4	8.1	28 ± 12	57.8
Trp	1.0	22 ± 5.6	64.6	7.7	>1000	53.2
HIV$_{N43D}$						
Ser	10.9	0.3 ± 0.1	69.9	7.4	2.0 ± 0.4	65.3
Ala	12.9	0.2 ± 0.1	74.4	10.2	0.3 ± 0.1	71.9
Leu	12.9[d]	0.2 ± 0.1	80.0	10.8[d]	0.2 ± 0.1	74.0
Pro	0.3	130 ± 52	55.6	0.3	430 ± 160	55.0
Thr	9.4	0.3 ± 0.1	67.5	6.1	3.7 ± 0.1	62.4
Trp	2.4	2.7 ± 0.6	66.0	7.6	220 ±17	61.4

[a] The recovery rate was determined from the relative detected signals of $[M + 3H]^{3+}$ and $[M + 4H]^{4+}$ ions by LC-MS analysis. [b] EC_{50} was determined as the concentration that blocked HIV-1_{NL4-3} replication by 50% in the MAGI assay. To improve the replication kinetics, the D36G mutation, observed in the majority of HIV-1 strains, was introduced into the NL4-3 background used in this study. [c] T_m values were defined by the midpoint of the thermal unfolding transition state measured by monitoring the molar ellipticity at 222 nm of N36$_{V38A}$/SC35EK$_{S138X}$, N36$_{N43D}$/SC35EK$_{S138X}$, N54$_{V38A}$/T-20EK$_{S138X}$ or N54$_{N43D}$/T-20EK$_{S138X}$ mixture. [d] Combined yield of 138I and 138L derivatives.

relationship of T-20EK$_{S138X}$ can be partially rationalized by the similar hydrophobic/hydrophilic properties of the side-chain. The recovery rates of T-20EK$_{S138X}$ in affinity selection showed good correlations with both anti-HIV activity and with thermal stability of the complexes (Fig. 3c and 3d). The peptides captured with more than 9% recovery yields exhibited sub-nanomolar potency along with T_m values >75 °C.

The anti-HIV activities of the series of peptides against recombinant viruses with either the enfuvirtide-resistant V38A or N43D mutation in N-HR were evaluated. The results of representative C-HR peptides, which were obtained by a single nucleotide mutation of HIV-1_{NL4-3}, are shown in Table 3 and Figure S2.† From Ser138 encoded by the TCG codon in wild-type NL4-3, Ala (GCG), Pro (CCG), Thr (ACG), Leu (TTG) and Trp (TGG) are possible mutations; the other mutations are silent (TCA, TCT, TCC) or a stop codon (TAG). The S138A substitution in both SC35EK and T-20EK enhanced the thermal stability of the N-HR/C-HR complex, indicating that this is a favorable mutation in terms of gp41 folding of the resistant virus.[3,4] These peptides by mutant-directed design restored and enhanced the anti-HIV activity against enfuvirtide-resistant variants. The S138L peptide was also effective against both V38A and N43D strains; however, no emergence of a clinical variant having this mutation has been reported. Of interest, resistant viruses are unlikely to necessarily use the best C-HR substitution to complement the gp41 folding, presumably due to the low replication kinetics. These results indicate that the mutations observed in clinical variants can direct the position to be optimized for inhibitor design but not the most appropriate amino acids. In practice, several other substitutions by Ile and Met, which are irrelevant to single nucleotide mutations from the wild-type, also provided potent anti-HIV activity against the resistant strains (Table S4, ESI†). In contrast, substitution with Pro or Trp for both peptides significantly decreased the activity,

Table 4 Peptide recovery in affinity selection, anti-HIV activity and thermal stability of the six-helix bundles of $SC35EK_{Q141X}$ and $T\text{-}20EK_{Q141X}$ derivatives

	$SC35EK_{Q141X}$			$T\text{-}20EK_{Q141X}$		
X	Recovery (%)[a]	EC_{50}/nM[b]	T_m/°C[c]	Recovery (%)[a]	EC_{50}/nM[b]	T_m/°C[c]
Gln	10.1	2.6 ± 0.3	81.6	8.2[e]	1.5 ± 0.6	78.8
Ala	6.6	1.6 ± 0.6	76.1	5.6	2.7 ± 0.3	70.4
Asp	4.5	2.9 ± 0.1	75.1	8.2	3.5 ± 0.7	71.4
Glu	4.3	2.4 ± 0.4	76.2	8.2[e]	3.8 ± 0.8	71.8
Phe	5.7	2.6 ± 0.4	76.7	5.3	2.6 ± 0.9	64.0
Gly	3.8	2.3 ± 0.7	71.0	3.4	3.0 ± 0.6	66.2
His	4.3	2.0 ± 0.5	72.6	3.7	3.0 ± 0.6	68.4
Ile	8.2[d]	2.9 ± 0.4	79.7	10.4[d]	0.8 ± 0.3	74.0
Lys	4.8	2.7 ± 0.5	69.2	4.8	3.8 ± 0.3	65.3
Leu	8.2[d]	2.7 ± 0.9	83.8	10.4[d]	0.5 ± 0.2	77.4
Met	6.0	2.0 ± 0.3	80.2	9.2	0.9 ± 0.1	74.6
Asn	4.0	2.5 ± 0.5	73.4	4.4	3.6 ± 0.7	69.0
Pro	0.0	58 ± 16	60.2	0.3	>1000	52.0
Arg	7.6	2.5 ± 0.1	71.5	7.2	1.5 ± 0.3	68.9
Ser	4.0	2.5 ± 0.7	72.4	3.2	4.6 ± 1.4	66.7
Thr	7.3	3.2 ± 0.6	76.7	6.9	2.1 ± 0.5	71.6
Val	6.2	2.2 ± 0.6	77.7	6.1	2.9 ± 0.2	70.5
Trp	7.1	1.7 ± 0.2	77.1	8.1	2.5 ± 0.1	68.8
Tyr	5.5	2.2 ± 0.6	76.3	4.9	2.3 ± 0.9	67.7

[a] The recovery rate was determined from the relative detected signals of $[M + 3H]^{3+}$ and $[M + 4H]^{4+}$ ions by LC-MS analysis. [b] EC_{50} was determined as the concentration that blocked $HIV\text{-}1_{NL4\text{-}3}$ replication by 50% in the MAGI assay. To improve the replication kinetics, the D36G mutation, observed in the majority of HIV-1 strains, was introduced into the NL4-3 background used in this study. [c] T_m values were defined by the midpoint of the thermal unfolding transition state measured by monitoring the molar ellipticity at 222 nm of $N36/SC35EK_{Q141}$ or $N54/T\text{-}20EK_{Q141}$ mixture. [d] Combined yield of 141I and 141L derivatives. [e] Combined yield of 141E and 141Q derivatives.

which is consistent with the results against the wild-type virus. Lower stabilities of the six-helical bundle structure consisting of S138T peptides and mutant N-HR peptides were shown, but $SC35EK_{S138T}$ was slightly more potent against both resistant viruses compared with the parent peptide.

Using His-tagged N36 or N54 peptides with the V38A or N43D mutation, affinity selection experiments were performed for $SC35EK_{S138X}$ and $T\text{-}20EK_{S138X}$ including 19 components (Table 3 and Table S4, ESI†). Eight SC35EK derivatives captured in significantly high yields all showed potent anti-HIV activity against the V38A mutant. Moderate recovery yields of $SC35EK_{S138E}$ and $SC35EK_{S138Y}$ could result from potential false positive and negative results of the selection, respectively. Although T-20EK derivatives showed lower susceptibility against the V38A mutant in the MAGI assay, an association between the high recovery rate and more potent anti-HIV activity was observed such as S138A, S138I, S138L and S138M derivatives (Figures S3, ESI†). Similar correlations were also obtained against N43D variants. $SC35EK_{S138X}$ and $T\text{-}20EK_{S138X}$ components, which exhibited subnanomolar potent bioactivity, were recovered in moderate to good yields. Overall favorable amino acids for position 138 of the wild-type were useful for designing C-HR peptides against V38A and N43D variants and *vice versa*, suggesting that the essential binding mode around this position is conserved even after acquiring the enfuvirtide resistance.

The structure–activity relationships of Q141 modifications were also investigated (Table 4). All $SC35EK_{Q141X}$ and $T\text{-}20EK_{Q141X}$ peptides except for the Q141P substitution exhibited similar anti-HIV activity in the EC_{50} range of 1.6–3.2 nM and 0.51–4.6 nM, respectively. The significantly low T_m values of Q141P derivatives suggested that the sole proline residue precluded the formation of a bioactive α-helix structure. On the other hand, high potency of the other peptides independent of any other acyclic amino acid substitution at position 141 may be attributable to the lower importance of the Q141 position for the binding affinity between N-HR and C-HR than the S138 position. Among these, Q141I, Q141L and Q141M peptides formed slightly more stable complexes with N36 or N54 and were captured at a relatively higher recovery rate by affinity selection. These substitutions were found to contribute to subnanomolar anti-HIV activity of T-20EK derivatives; however, these peptides were less valid for SC35EK derivatives.

For both S138 and Q141 substitutions, it does not seem possible to distinguish between variations of a few nM in anti-HIV activity by affinity selection. This is particularly the case for the selections regarding less effective residues such as Q141 of SC35EK. In contrast, over a larger range of more than 2 orders of magnitude of affinity variations of T-20EK derivatives, the selection procedure correlated reasonably well with the anti-HIV activity and six-helix bundle stability. In both sequences, highly potent anti-HIV activity peptides were captured in good to high yields.

Conclusions

In conclusion, we have presented an affinity selection-mass spectrometry method to explore novel HIV-1 fusion inhibitors. Predicated on previous findings that the introduction of α-helix-inducible X-EE-XX-KK motifs into inhibitory C-HR peptides should improve peptide solubility in aqueous buffers and disclose the interactive surface to be optimized, a pool of SC35EK and T-20EK derivatives with a single modification at two interactive positions were screened using N-HR peptides corresponding to

wild-type and enfuvirtide-resistant strains. Through the screening of position 138 on C-HR, it was demonstrated that potent anti-HIV peptides could be obtained by substitutions with resistance-related and resistance-independent amino acids. Since a wide variety of synthetic peptides with any unnatural amino acids or peptidomimetics could be employed as candidate components, the system should be applicable to screening for inhibitory α-helix peptides of coiled-coil interactions. The structure–activity relationships of C-HR peptides presented herein may also be suitable in the design of the next-generation of fusion inhibitors. Additionally, since this process is considered to reproduce the evolutionary process of HIV-1 gp41 to select the appropriate folding partners in the presence of fusion inhibitors, the sequence-activity relationships could facilitate understanding of the underlying mechanisms of enfuvirtide resistance.

Acknowledgements

This work was supported by the Science and Technology Incubation Program in Advanced Regions from the Japan Science and Technology Agency, Grants-in-Aid for Scientific Research and Targeted Proteins Research Program from the Ministry of Education, Culture, Sports, Science, and Technology of Japan, and Health and Labour Sciences Research Grants (Research on HIV/AIDS). H.N. is grateful for the JSPS Research Fellowships for Young Scientists.

References

1 T. Matthews, M. Salgo, M. Greenberg, J. Chung, R. DeMasi and D. Bolognesi, *Nat. Rev. Drug Discovery*, 2004, **3**, 215–225.
2 D. C. Chan, C. T. Chutkowski and P. S. Kim, *Proc. Natl. Acad. Sci. U. S. A.*, 1998, **95**, 15613–15617.
3 L. Xu, A. Pozniak, A. Wildfire, S. A. Stanfield-Oakley, S. M. Mosier, D. Ratcliffe, J. Workman, A. Joall, R. Myers, E. Smit, P. A. Cane, M. L. Greenberg and D. Pillay, *Antimicrob. Agents Chemother.*, 2005, **49**, 1113–1119.
4 L. Pérez-Alvarez, R. Carmona, A. Ocampo, A. Asorey, C. Miralles, S. Pérez de Castro, M. Pinilla, G. Contreras, J. A. Taboada and R. Nájera, *J. Med. Virol.*, 2006, **78**, 141–147.
5 D. Eggink, J. P. Langedijk, A. M. Bonvin, Y. Deng, M. Lu, B. Berkhout and R. W. Sanders, *J. Biol. Chem.*, 2009, **284**, 26941–26950.
6 D. Nameki, E. Kodama, M. Ikeuchi, N. Mabuchi, A. Otaka, H. Tamamura, M. Ohno, N. Fujii and M. Matsuoka, *J. Virol.*, 2005, **79**, 764–770.
7 D. C. Chan, D. Fass, J. M. Berger and P. S. Kim, Core structure of gp41 from the HIV envelope glycoprotein, *Cell*, 1997, **89**, 263–273.
8 T. Watabe, Y. Terakawa, K. Watanabe, H. Ohno, H. Nakano, T. Nakatsu, H. Kato, K. Izumi, E. Kodama, M. Matsuoka, K. Kitaura, S. Oishi and N. Fujii, *J. Mol. Biol.*, 2009, **392**, 657–665.
9 K. Izumi, S. Nakamura, H. Nakano, K. Shimura, Y. Sakagami, S. Oishi, S. Uchiyama, T. Ohkubo, Y. Kobayashi, N. Fujii, M. Matsuoka and E. N. Kodama, *Antiviral Res.*, 2010, **87**, 179–186.
10 J. P. Lalezari, N. C. Bellos, K. Sathasivam, G. J. Richmond, C. J. Cohen, R. A. Myers, Jr., D. H. Henry, C. Raskino, T. Melby, H. Murchison, Y. Zhang, R. Spence, M. L. Greenberg, R. A. Demasi and G. D. Miralles, *J. Infect. Dis.*, 2005, **191**, 1155–1163.
11 Y. He, Y. Xiao, H. Song, Q. Liang, D. Ju, X. Chen, H. Lu, W. Jing, S. Jiang and L. Zhang, *J. Biol. Chem.*, 2008, **283**, 11126–11134.
12 K. Izumi, E. Kodama, K. Shimura, Y. Sakagami, K. Watanabe, S. Ito, T. Watabe, Y. Terakawa, H. Nishikawa, S. G. Sarafianos, K. Kitaura, S. Oishi, N. Fujii and M. Matsuoka, *J. Biol. Chem.*, 2008, **284**, 4914–4920.
13 J. Cao, L. Bergeron, E. Helseth, M. Thali, H. Repke and J. Sodroski, *J. Virol.*, 1993, **67**, 2747–2755.
14 W. Shu, J. Liu, H. Ji, L. Radigen, S. Jiang and M. Lu, *Biochemistry*, 2000, **39**, 1634–1642.
15 D. A. Annis, N. Nazef, C. C. Chuang, M. P. Scott and H. M. Nash, *J. Am. Chem. Soc.*, 2004, **126**, 15495–15503.
16 G. C. Adam, C. A. Parish, D. Wisniewski, J. Meng, M. Liu, K. Calati, B. D. Stein, J. Athanasopoulos, P. Liberator, T. Roemer, G. Harris and K. T. Chapman, *J. Am. Chem. Soc.*, 2008, **130**, 16704–16710.
17 S. Oishi, S. Ito, H. Nishikawa, K. Watanabe, M. Tanaka, H. Ohno, K. Izumi, Y. Sakagami, E. Kodama, M. Matsuoka and N. Fujii, *J. Med. Chem.*, 2008, **51**, 388–391.
18 A. Otaka, M. Nakamura, D. Nameki, E. Kodama, S. Uchiyama, S. Nakamura, H. Nakano, H. Tamamura, Y. Kobayashi, M. Matsuoka and N. Fujii, *Angew. Chem., Int. Ed.*, 2002, **41**, 2937–2940.
19 M. Gochin, R. Savage, S. Hinckley and L. Cai, *Biol. Chem.*, 2006, **387**, 477–483.
20 H. Nishikawa, E. Kodama, A. Sakakibara, A. Fukudome, K. Izumi, S. Oishi, N. Fujii and M. Matsuoka, *Antiviral Res.*, 2008, **80**, 71–76.
21 J. K. Judice, J. Y. Tom, W. Huang, T. Wrin, J. Vennari, C. J. Petropoulos and R. S. McDowell, *Proc. Natl. Acad. Sci. U. S. A.*, 1997, **94**, 13426–13430.
22 S. K. Sia, P. A. Carr, A. G. Cochran, V. N. Malashkevich and P. S. Kim, *Proc. Natl. Acad. Sci. U. S. A.*, 2002, **99**, 14664–14669.
23 J. J. Dwyer, K. L. Wilson, D. K. Davison, S. A. Freel, J. E. Seedorff, S. A. Wring, N. A. Tvermoes, T. J. Matthews, M. L. Greenberg and M. K. Delmedico, *Proc. Natl. Acad. Sci. U. S. A.*, 2007, **104**, 12772–12777.

Immunity
Article

The Essential Functions of Adipo-osteogenic Progenitors as the Hematopoietic Stem and Progenitor Cell Niche

Yoshiki Omatsu,[1] Tatsuki Sugiyama,[1] Hiroshi Kohara,[1] Gen Kondoh,[2] Nobutaka Fujii,[3] Kenji Kohno,[4] and Takashi Nagasawa[1,*]
[1]Department of Immunobiology and Hematology
[2]Laboratory of Animal Experiments for Regeneration, Institute for Frontier Medical Sciences
Kyoto University, 53 Kawahara-cho, Shogoin, Sakyo-ku, Kyoto 606-8507, Japan
[3]Graduate School of Pharmaceutical Sciences, Kyoto University, Sakyo-ku, Kyoto 606-8501, Japan
[4]Laboratory of Molecular and Cell Genetics, Graduate School of Biological Sciences, Nara Institute of Science and Technology (NAIST), 8916-5 Takayama, Ikoma, Nara 630-0192, Japan
*Correspondence: tnagasa@frontier.kyoto-u.ac.jp
DOI 10.1016/j.immuni.2010.08.017

SUMMARY

Hematopoietic stem cells (HSCs) and their lympho-hematopoietic progeny are supported by microenvironmental niches within bone marrow; however, the identity, nature, and function of these niches remain unclear. Short-term ablation of CXC chemokine ligand (CXCL)12-abundant reticular (CAR) cells in vivo did not affect the candidate niches, bone-lining osteoblasts, or endothelial cells but severely impaired the adipogenic and osteogenic differentiation potential of marrow cells and production of the cytokines SCF and CXCL12 and led to a marked reduction in cycling lymphoid and erythroid progenitors. HSCs from CAR cell-depleted mice were reduced in number and cell size, were more quiescent, and had increased expression of early myeloid selector genes, similar to the phenotype of wild-type HSCs cultured without a niche. Thus, the niche composed of adipo-osteogenic progenitors is required for proliferation of HSCs and lymphoid and erythroid progenitors, as well as maintenance of HSCs in an undifferentiated state.

INTRODUCTION

Hematopoietic stem cells (HSCs) give rise to all lineages of blood cells, including immune cells in the bone marrow. It has been assumed that the special microenvironments known as niches play an essential role in maintaining HSCs and hematopoietic progenitors in the marrow to provide appropriate numbers of mature blood cells throughout life (Morrison and Spradling, 2008; Wilson and Trumpp, 2006). HSCs and lymphoid progenitors are thought to reside in their niches, and the identity of the niche has been a subject of longstanding debate. It has been shown that HSCs are in contact with a population of osteoblasts lining the bone surface, termed spindle-shaped N-cadherin^{+}CD45^{-} osteoblastic (SNO) cells, which express a high amount of N-cadherin (endosteal niches) (Zhang et al., 2003). In contrast, many HSCs are associated with sinusoidal endothelium, suggesting that endothelial cells create cellular niches for HSCs (vascular niches) (Kiel et al., 2005). We have shown that CXCR4, a primary receptor for the CXC chemokine ligand (CXCL)12 (also known as stromal cell-derived factor-1) (Nagasawa, 2006; Nagasawa et al., 1996; Nagasawa et al., 1994; Tachibana et al., 1998; Zou et al., 1998), is essential for maintaining a pool of HSCs and B cells and that most HSCs, early B cell precursors, and plasma cells are scattered throughout the bone marrow cavity and are in contact with a small population of reticular cells with long processes, expressing high amounts of CXCL12, called CXCL12-abundant reticular (CAR) cells, suggesting that CAR cells are a key component of niches for both HSCs and B cells (Nagasawa, 2008; Sugiyama et al., 2006; Tokoyoda et al., 2004). However, these studies do not reveal the functions of SNO cells, endothelial cells, and CAR cells as niches for HSCs and/or lymphoid progenitors.

Prior studies using a variety of gain-of-function and loss-of-function approaches examined the identity and functions of cellular niches for HSCs and hematopoietic progenitors. Bone morphogenetic protein (BMP) receptor type IA (BMPRIA) conditionally deficient mice displayed increases in the numbers of SNO cells, which correlated with an increase in the numbers of HSCs (Zhang et al., 2003). Parathyroid hormone (PTH) administration increased the numbers of osteoblasts in culture and induced an increase in the number of HSCs in vivo (Calvi et al., 2003). In contrast, it has been shown that depleting osteoblastic lineage cells with a 2.3 kb fragment from the rat type I collagen α1 (Col1α1) gene promoter driving thymidine kinase (Col2.3ΔTK) induced a marked reduction in hematopoietic cells (Visnjic et al., 2004; Zhu et al., 2007). These results suggest that osteoblastic lineage cells maintain HSCs and hematopoietic cells but do not rule out the possibility that Col1α1, BMPRIA, and PTH or PTH-related protein receptor (PPR) are expressed in bone marrow reticular cells, including CAR cells. In addition, it has been reported that reductions in osteoblasts do not necessarily lead to reductions in HSCs and hematopoietic cells (Kiel et al., 2007; Wilson and Trumpp, 2006). Together, it remains unresolved which cell types play major roles in regulating the

maintenance of HSCs and lymphoid progenitors within bone marrow.

It is assumed that most adult HSCs are quiescent and that HSC quiescence is maintained by their niches (Arai et al., 2004; Orford and Scadden, 2008). In contrast, many studies have shown that the majority of HSCs are cycling, albeit slowly, although some HSCs are highly dormant, (Cheshier et al., 1999; Foudi et al., 2009; Santaguida et al., 2009; Wilson et al., 2008; Yamazaki et al., 2006) and that many lineage-restricted progenitors are known to be cycling actively, supporting the idea that HSC and hematopoietic progenitor proliferation is maintained by their niches. However, the technology to prove this was lacking and the role of niches in controlling the quiescence, proliferation, and differentiation of HSCs and lymphoid progenitors remain unclear. Here, we generated mice that allow selective ablation of CAR cells in bone marrow and determined the nature and in vivo function of CAR cells as a niche for HSCs and lympho-hematopoietic progenitors.

RESULTS

Generation of Mice that Allow Inducible Selective Ablation of CAR Cells In Vivo

To determine the nature and in vivo function of CAR cells, we generated mice in which a transgene encoding the Diphtheria toxin (DT) receptor-green fluorescent protein (DTR-GFP) fusion protein (Saito et al., 2001) was knocked into the *Cxcl12* locus (CXCL12-DTR-GFP mice) (Figure 1A). These mice allow the conditional ablation of CXCL12-expressing cells by DT administration because wild-type murine cells are insensitive to killing by DT (Saito et al., 2001). CXCL12-DTR-GFP mice were injected intraperitoneally (i.p.) with DT at a dose of 25 ng/kg; many mice remained healthy for up to 3 days after injection and died 5 days after injection probably from liver failure. By histological analysis, the liver of CXCL12-DTR-GFP mice showed necrosis and haemorrhage at 5 days after DT treatment but appeared normal at 2 days after DT treatment. Histological analysis of bone marrow microenvironments 2 or 3 days after DT treatment revealed that CXCL12-DTR-GFP$^+$ CAR cells were eliminated or severely reduced, but bone-lining SNO cells, osteocalcin$^+$ or marked alkaline phosphatase (ALP) activity-containing osteoblasts, and sinusoidal endothelial cells remained unaffected in DT-treated CXCL12-DTR-GFP mice compared with untreated CXCL12-DTR-GFP mice (Figures 1B and 1C; Figure S1 available online; data not shown). Flow-cytometric analysis confirmed that the numbers of CXCL12-DTR-GFP^{hi} CAR cells were severely reduced in DT-treated CXCL12-DTR-GFP mice compared with untreated animals (Figure 1E). In addition, consistent with the result that CAR cells are a small population of VCAM-1$^+$ reticular cells (Tokoyoda et al., 2004), many VCAM-1$^+$ reticular cells were observed in DT-treated and untreated CXCL12-DTR-GFP mice (Figure 1D).

Short-Term Ablation of CAR Cells Leads to a Reduction in Cycling Lymphoid and Erythroid Progenitors

To better define the direct effect of CAR cell depletion on hematopoiesis, we examined the effect of short-term ablation of CAR cells on hematopoietic cells in the bone marrow using CXCL12-DTR-GFP mice 2 days after DT treatment, in which CAR cells were eliminated or severely reduced. Total bone marrow cellularity was reduced in DT-treated CXCL12-DTR-GFP mice compared with DT-treated and untreated wild-type mice (Figure 2A and Figure S2A). Flow-cytometric analysis of hematopoietic progenitors revealed that although the numbers of Lineage(Lin)$^-$Sca-1$^+$c-kit$^+$Flt3$^+$ multipotent progenitors (MPPs) (Adolfsson et al., 2001) appeared normal, Lin$^-$IL-7Rα^+Flt3$^+$ common lymphoid progenitors (CLPs) (Karsunky et al., 2008) and c-kit$^+$CD71$^+$Ter119^{lo} proerythroblasts were almost absent, the numbers of c-kit$^+$CD19$^+$IgM$^-$ pro-B cells and Lin$^-$Sca-1$^-$c-kit$^+$CD34$^-$FcγRII-III^{lo} megakaryocyte and erythrocyte progenitors (MEPs) (Akashi et al., 2000) were severely reduced and the number of Lin$^-$Sca-1$^-$c-kit$^+$CD34$^+$FcγRII-III^{hi} granulocyte and macrophage progenitors (GMPs) (Akashi et al., 2000) was more modestly reduced in DT-treated CXCL12-DTR-GFP mice compared with untreated CXCL12-DTR-GFP mice or DT-treated and untreated wild-type mice (Figures 2B and 2C and Figure S2A). Cell-cycle analysis of pro-B cells and MEPs using Pyronin Y (PY) revealed that around half of the cells were cycling actively (high PY fluorescence [PY^{hi}]) and other quiescent cells displayed low PY fluorescence (PY^{lo}) in DT-treated wild-type mice. In contrast, a reduction in the frequency of PY^{hi} cells and an increase in the frequency of PY^{lo} cells were observed in DT-treated CXCL12-DTR-GFP mice (Figure 2D). Additionally, Annexin-V staining of pro-B cells revealed many apoptotic cells (43%) in DT-treated CXCL12-DTR-GFP mice although few (5.1%) were detected in DT-treated wild-type mice (Figure 2E). These results indicate that CAR cells are essential for lymphoid, erythroid, and myeloid lineage development and suggest that CAR cells support the survival and proliferation of B cell progenitors and proliferation of erythroid progenitors.

HSCs Are Reduced and More Quiescent in the Absence of CAR Cells

We next examined the effect of short-term ablation of CAR cells on HSCs. Bone marrow from CXCL12-DTR-GFP and wild-type mice was analyzed 2 days after DT treatment. The number of CD34$^-$Lin$^-$Sca-1$^+$c-kit$^+$CD150$^+$CD48$^-$ cells, which are highly enriched for long-term repopulating HSCs (Foudi et al., 2009; Kiel et al., 2005; Wilson et al., 2008), was reduced, but to a lesser extent than lymphoid and erythroid progenitors in DT-treated CXCL12-DTR-GFP mice compared with control animals (Figure 3A and Figure S3A). Because the unambiguous measure of HSCs is long-term transplantation, we estimated the numbers of HSCs using repopulating units (RU), based on a competitive repopulation assay (Harrison et al., 1993). The numbers of RU were reduced about 50% in the bone marrow of CXCL12-DTR-GFP mice compared with wild-type mice (Figure 3B), indicating that CAR cells play an essential role in maintaining the HSC number.

Flow-cytometric analysis using the proliferation marker Ki67 has shown that a small percentage of CD34$^-$Lin$^-$Sca-1$^+$c-kit$^+$CD48$^-$ HSCs express Ki67 in DT-treated or untreated wild-type mice, as reported previously, but the numbers of Ki67-positive cells were severely reduced in the HSC population from DT-treated CXCL12-DTR-GFP mice (Figure 3C). Quantitative, real-time polymerase chain reaction with reverse transcription (qRT-PCR) analysis revealed that the mRNA expression of Evi-1 and Pbx1, which are essential for HSC maintenance and

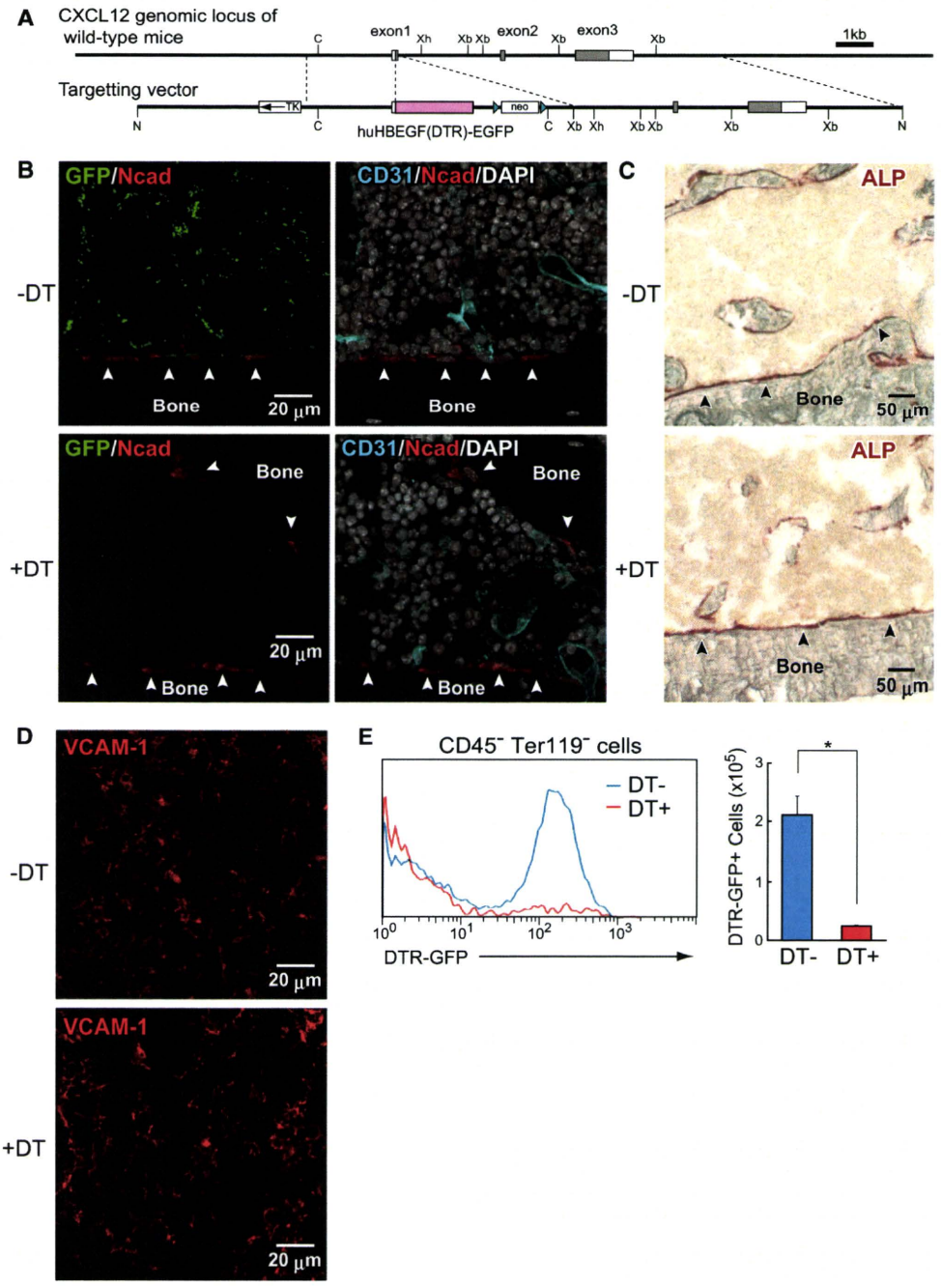

Figure 1. Short-Term Selective Ablation of CAR Cells In Vivo in Bone Marrow

(A) Strategy used to generate CXCL12-DTR-GFP mice. C, Csp45I; Xh, XhoI; Xb, XbaI; N, NotI. Triangles represent LoxP sites.

(B–E) Bone marrow from CXCL12-DTR-GFP mice was analyzed 2 days after administration of DT or control vehicle. Bone marrow sections were stained with antibodies against GFP, N-cadherin, the panendothelial marker PECAM-1 (CD31) (B), and VCAM-1 (D) and assayed by Fast Red staining (C). CXCL12-DTR-GFP^{+} CAR cells (green) are eliminated (B, left); however, bone-lining SNO cells detected by anti-N-cadherin antibodies (B, arrowheads; red), marked ALP activity-containing osteoblasts (C, arrowheads; red), and sinusoidal endothelial cells (B, right; blue) exhibit normal numbers and morphology in DT-treated CXCL12-DTR-GFP mice. The nuclei of cells were labeled with DAPI dye (B, right; white). (E) Flow cytometric analysis of CD45^{-}Ter119^{-}CD31^{-} nonhematopoietic cells. The numbers of CXCL12-DTR-GFP^{hi} CAR cells per two femurs and tibiae are shown (E, right). All error bars represent SD of the mean. n = 4; *p < 0.05.

preferentially expressed in HSCs (Ficara et al., 2008; Goyama et al., 2008), was largely unaffected in the HSC population from DT-treated CXCL12-DTR-GFP mice (Figure 3D and Figure S3C). In contrast, although cell-cycle-promoting genes, including those that encode Cyclin D1, D2, A2, and their catalytic partner, Cdc2a, and a regulator of initiation of DNA replication, Cdc6, were expressed in the HSC population from DT-treated and untreated wild-type mice and untreated CXCL12-DTR-GFP

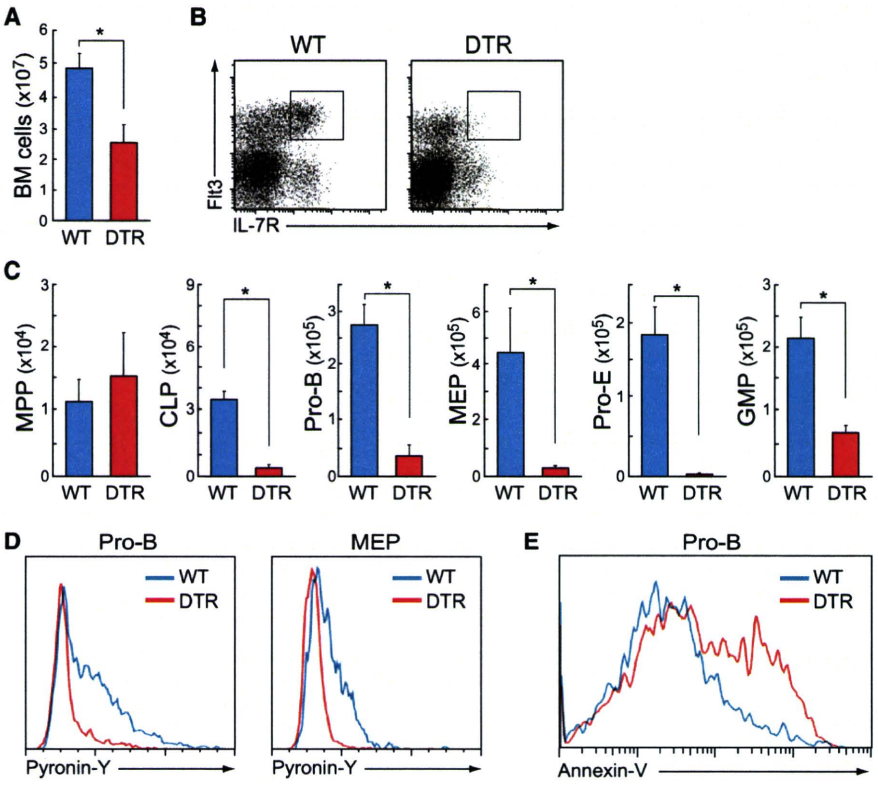

Figure 2. Essential In Vivo Functional Roles of CAR Cells in Lympho-hematopoietic Progenitors

Bone marrow from wild-type and CXCL12-DTR-GFP mice was analyzed by flow cytometry 2 days after DT administration.

(A) Total numbers of $CD45^+$ hematopoietic cells per two femurs and tibiae. n = 3; *p < 0.05.

(B) Immunofluorescent profiles of CLPs. Gated Lin^- cells are analyzed for the expression of IL-7Rα and Flt3.

(C) The numbers of MPPs, CLPs, pro-B cells, MEPs, proerythroblasts (pro-E), and GMPs per two femurs and tibiae. n = 3; *p < 0.05.

(D) RNA content of pro-B cells and MEPs by PY staining.

(E) Annexin-V staining of pro-B cells.

All error bars represent SD of the mean (A and C).

mice, consistent with previous studies (Kalaszczynska et al., 2009; Kozar et al., 2004; Santaguida et al., 2009; Yamazaki et al., 2006), expression of these genes was markedly reduced in the HSC population from DT-treated CXCL12-DTR-GFP mice (Figure 3D and data not shown). In addition, mRNA expression of the transcriptional repressor Mad1, considered to decrease cell size (Iritani et al., 2002) and inhibit HSC proliferation (Walkley et al., 2005), was significantly elevated in the HSC population from DT-treated CXCL12-DTR-GFP mice (Figure 3D). Cellular activation by growth factors induces entry into a phase of cell cycle characterized by initiation of transcription and accumulation of RNA, mainly in the form of ribosomal RNA, which can be measured by RNA-specific dyes, such as PY. As reported previously, almost all $CD34^-Lin^-Sca\text{-}1^+$ $c\text{-}kit^+CD48^-$ HSCs from DT-treated wild-type mice displayed low PY fluorescence (Figure 3E); however, PY fluorescence in many HSCs from DT-treated CXCL12-DTR-GFP mice decreased further compared with wild-type mice (Figure 3E). Furthermore, in DT-treated CXCL12-DTR-GFP mice, most cells in the HSC population were smaller than those in control animals, shown by forward scatter characteristics (FSCs) on flow cytometry, although Annexin-V staining revealed no increase in apoptotic cells in the population (Figure 3F and Figure S3D). Histological analysis of the bone marrow from DT-treated CXCL12-DTR-GFP mice, in which CAR cells were severely reduced, revealed that $CD150^+CD48^-CD41^-$ HSCs, which did not adjoin CAR cells, were significantly smaller than HSCs in contact with the processes of residual CAR cells, indicating that short-term ablation of CAR cells leads to a significant decrease in the cell size of adjacent HSCs (Figures 3G and 3H).

Together, these results indicate that HSCs are more quiescent in CAR cell-depleted mice and that CAR cells keep HSCs in a proliferative state.

Short-Term Ablation of CAR Cells Induces Early Myeloid Differentiation of HSCs

It is unclear whether HSC niches regulate the differentiation of HSCs. To address this issue, we analyzed the expression of genes that encode activities important for HSC differentiation in the HSC population from CAR cell-depleted mice. It has been shown that elevating the expression of transcription factor PU.1 in primitive multipotent progenitors induces the generation of myeloid lineage (Arinobu et al., 2007; DeKoter and Singh, 2000). Of note, qRT-PCR analysis revealed that the mRNA expression of PU.1 and its macrophage-specific target M-CSF receptor (M-CSFR) was markedly increased in the $CD34^-Lin^-Sca\text{-}1^+c\text{-}kit^+CD150^+$ $CD48^-$ HSC population from CXCL12-DTR-GFP mice 2 days after DT treatment, compared with untreated CXCL12-DTR-GFP mice or DT-treated and untreated wild-type mice (Figure 3I and data not shown).

Cells in the HSC population were sorted from bone marrow of wild-type and CXCL12-DTR-GFP mice 2 days after DT treatment and cultured in the presence of SCF and CXCL12, which support myeloid differentiation from HSCs and more mature multipotent progenitors. Flow-cytometric analysis showed that substantial numbers of $Gr\text{-}1^{hi}CD11b^+$ myeloid lineage cells were generated from wild-type HSCs at day 10 of culture and peaked at day 14 or later (data not shown). In contrast, cells in the HSC population from CAR cell-depleted mice had generated substantial numbers of $Gr\text{-}1^{hi}CD11b^+$ myeloid lineage cells earlier, day 7 of culture, and peaked at day 10, supporting the idea that some cells in the HSC population from CAR cell-depleted mice are more differentiated than in wild-type mice (Figure 3J and data not shown). Together, these results suggest that short-term CAR cell depletion prevented HSC maintenance in an undifferentiated state.

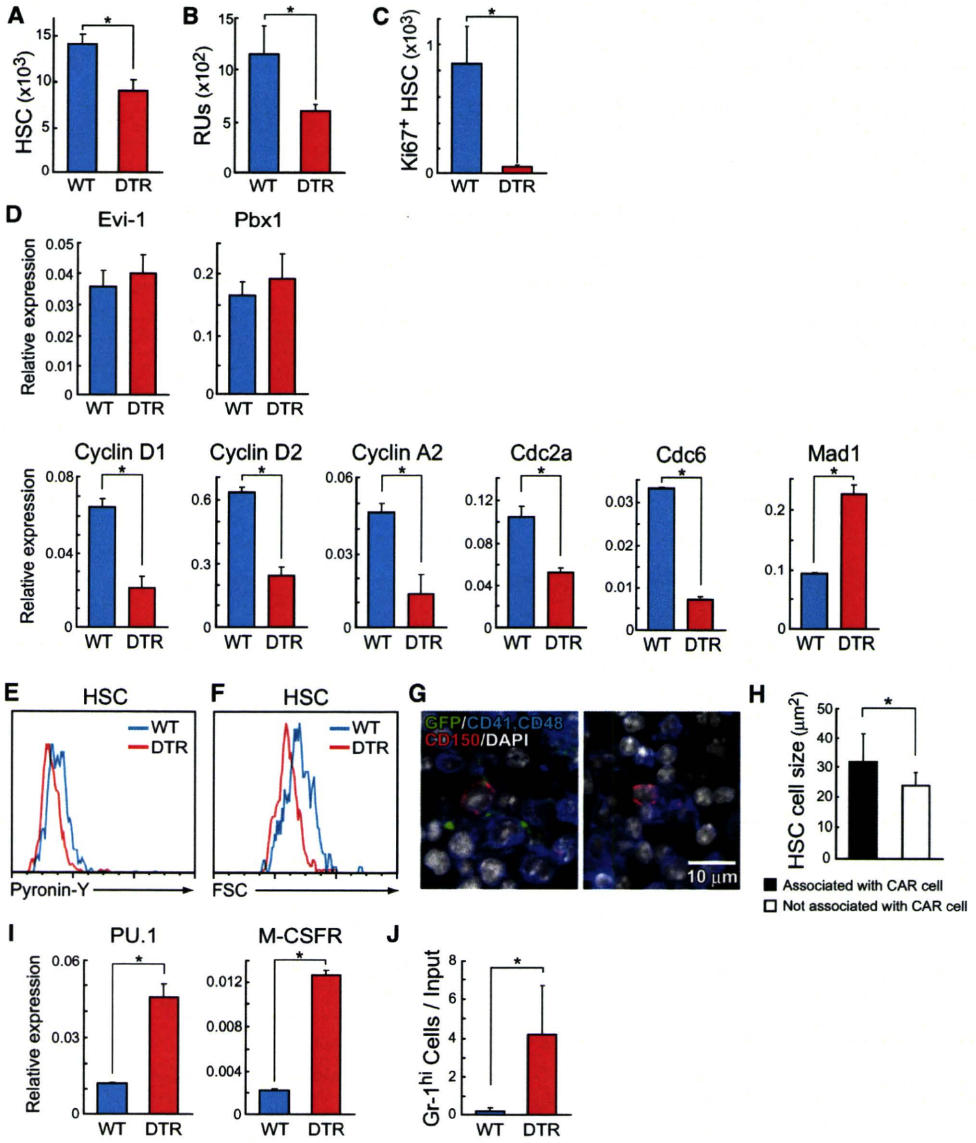

Figure 3. Essential In Vivo Functional Roles of CAR Cells in HSCs

Bone marrow from wild-type and CXCL12-DTR-GFP mice was analyzed 2 days after DT administration.

(A) Flow-cytometric analysis of the numbers of cells in the CD34$^-$Lin$^-$Sca-1$^+$c-kit$^+$CD150$^+$CD48$^-$ HSC population per two femurs and tibiae. n = 3; *p < 0.05.

(B) The numbers of HSCs were estimated using repopulating units (RU), based on a competitive repopulation assay. n = 3; *p < 0.05.

(C) Flow-cytometric analysis of the numbers of Ki67-positive cells in the HSC population per two femurs and tibiae. n = 3; *p < 0.05.

(D) Relative mRNA expression levels of Evi-1, Pbx1, Cyclin D1, D2, A2, Cdc2a, Cdc6, and Mad1 in sorted cells in the HSC population by qRT-PCR analysis normalized to G3PDH levels. n = 4; *p < 0.05.

(E) Flow-cytometric analysis of RNA content of cells in the HSC population by PY staining.

(F) Flow-cytometric analysis of cell size of cells in the HSC population by FSC.

(G and H) Sections of bone marrow from DT-treated CXCL12-DTR-GFP mice were stained with antibodies against CD150, CD48, and CD41. Cell size of CD150$^+$CD48$^-$CD41$^-$ HSCs in contact with (G, left) or at a distance from remaining CAR cells (G, right) was determined using a confocal microscope and its software (H). n = 20; *p < 0.05.

(I) Relative mRNA expression levels of PU.1 and M-CSFR in sorted cells in the HSC population by qRT-PCR analysis normalized to G3PDH levels. n = 4; *p < 0.05.

(J) Generation of myeloid lineage cells from cells in the HSC population in culture at an early point of time. Sorted cells in the HSC population were cultured in the presence of SCF and CXCL12. Flow-cytometric analysis of the numbers of Gr-1^{hi}CD11b$^+$ cells per input cell at day 7 of culture. n = 4; *p < 0.05. All error bars represent SD of the mean (A–D and H–J).

DT Does Not Act Directly on Hematopoietic Cells in CXCL12-DTR-GFP Mice

To rule out the possibility that DT acted directly on hematopoietic cells in DT-treated CXCL12-DTR-GFP mice, we infused bone marrow cells from CXCL12-DTR-GFP or wild-type mice into lethally irradiated recipients in the absence of competitor cells. When bone marrow hematopoietic cells of chimeric mice were mainly derived from donor HSCs 12 weeks after transplantation,

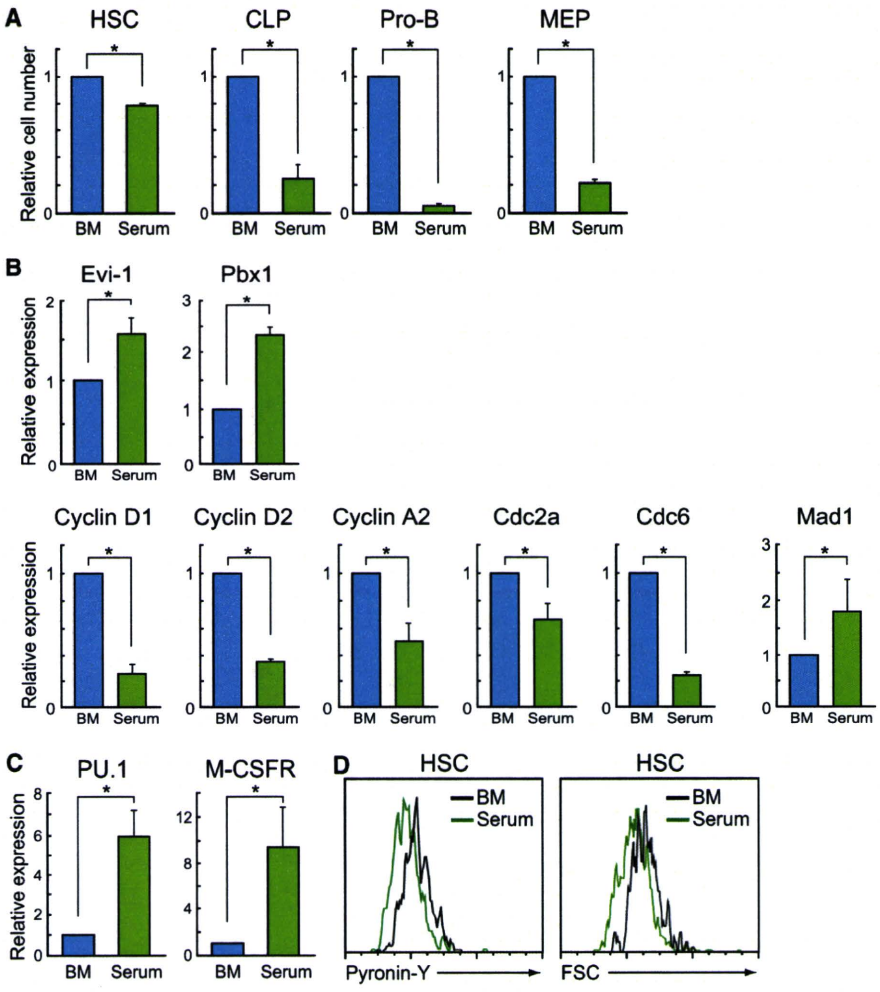

Figure 4. The Phenotypes of Wild-Type HSCs and Lympho-hematopoietic Progenitors Cultured in Serum Alone

(A) Single $CD34^-Lin^-Sca\text{-}1^+c\text{-}kit^+CD150^+CD48^-$ HSCs, CLPs, pro-B cells, and MEPs from wild-type mice were sorted and cultured in serum alone (1 cell/well). The numbers of living cells after 48 hr culture are shown (green bars). Control samples before culture have been normalized to 1. n = 3; $^*p < 0.05$.

(B–D) $CD34^-Lin^-Sca\text{-}1^+c\text{-}kit^+CD150^+CD48^-$ HSCs from wild-type mice were sorted and cultured in serum alone. QRT-PCR analysis of mRNA expression of HSC-specific genes (B, upper) and genes involved in cell-cycle promotion or repression (B, lower) and early myeloid differentiation (C) in HSCs before and after 6 hr culture. Results are expressed as fold difference compared to the levels found in freshly isolated HSCs from wild-type mice (G3PDH normalization). n = 3; $^*p < 0.05$.

(D) Left: flow-cytometric analysis of RNA content of HSCs before (black line) and after (green line) 6 hr culture by PY staining. Right: flow-cytometric analysis of cell size of HSCs before (black line) and after (green line) 12 hr culture by PY staining by FSC. All error bars represent SD of the mean (A–C).

we injected these chimeric mice with 100 ng/kg DT. Flow-cytometric analysis revealed that the numbers of donor-derived $CD34^-Lin^-Sca\text{-}1^+c\text{-}kit^+CD150^+CD48^-$ HSCs, CLPs, pro-B cells, MEPs, proerythroblasts, and GMPs, and the cell size of donor-derived HSCs in mutant chimeras, were comparable to those observed in control chimeras 2 days after DT treatment (Figures S2B and S3B). These results indicate that a 4-fold excess of DT does not act directly on CXCL12-DTR-GFP hematopoietic cells and that the failure of hematopoiesis in DT-treated CXCL12-DTR-GFP mice was because of environmental factors.

Phenotypes of HSCs Cultured in Serum Are Similar to Those from CAR Cell-Depleted Mice

To confirm further the role of bone marrow niches for HSCs and lymphoid and erythroid progenitors, we sorted $CD34^-Lin^-Sca\text{-}1^+c\text{-}kit^+CD150^+CD48^-$ HSCs, CLPs, pro-B cells, and MEPs from bone marrow of wild-type mice and cultured them in serum alone. After 48 hr of single-cell cultures, many HSCs remained viable, but the numbers of living CLPs, pro-B cells, and MEPs were progressively decreased over time (Figure 4A). QRT-PCR analysis revealed that the mRNA expression of Cyclin D1, D2, A2, Cdc2a, and Cdc6 was significantly reduced, although the mRNA expression of Evi-1, Pbx1, and Mad1 was elevated in the HSC population after 6 hr of culture (Figure 4B). In addition, the mRNA expression of PU.1 and M-CSFR was markedly increased in the HSC population cultured in serum alone (Figure 4C). Flow-cytometric analysis of cultured HSCs revealed that PY fluorescence and the cell size was decreased compared with freshly isolated HSCs, although Annexin-V staining revealed no significant increase in apoptotic cells (Figure 4D and Figure S4). Together, these results demonstrate that phenotypes of wild-type HSCs and lymphoid and erythroid progenitors cultured in serum alone were similar to those from CAR cell-depleted bone marrow.

CAR Cells Are the Major Producer of SCF as Well as CXCL12 in Bone Marrow

To determine the mechanism by which CAR cells support HSCs and hematopoietic progenitors, we compared the mRNA expression of SCF and CXCL12, which are essential for the maintenance of HSCs, CLPs, and B cell and erythroid progenitors (Kohara et al., 2007; Miller et al., 1996; Sugiyama et al., 2006; Tokoyoda et al., 2004; Waskow et al., 2002), in CAR cells to other microenvironmental components of bone marrow. Flow-cytometric analysis of CXCL12-GFP mice has shown that CAR cells ($CXCL12\text{-}GFP^{hi}VCAM\text{-}1^+CD45^-Ter119^-$) constitute approximately 0.27% of nucleated cells in the bone marrow fraction. In the bone fraction, some $CD45^-Ter119^-$ nonhematopoietic cells have a much lower expression of CXCL12-GFP relative to CAR cells, and osteopontin $(OPN)^+$ cells have been reported to include osteoblastic niche cells (Mayack and Wagers, 2008). QRT-PCR analysis of sorted CAR cells, $CD31^+Sca\text{-}1^+CD45^-Ter119^-$ endothelial cells, and

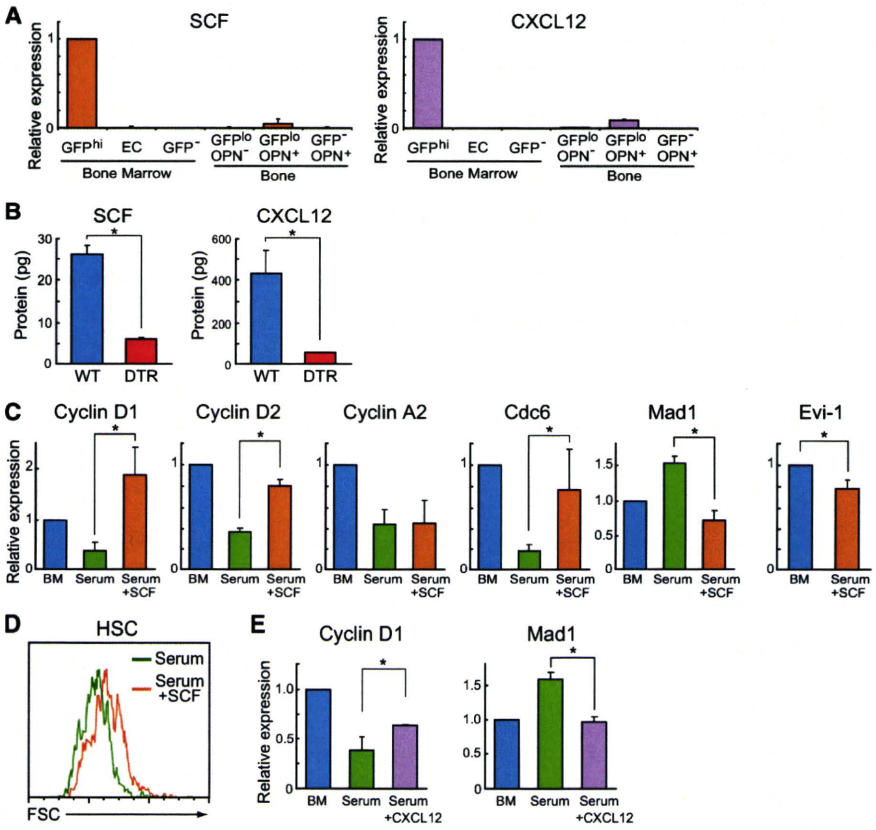

Figure 5. Preferential Expression of SCF and CXCL12 in CAR Cells

(A) QRT-PCR analysis of mRNA expression of SCF and CXCL12 in sorted CXCL12-GFP^{hi} CD45$^-$Ter119$^-$ CAR cells, CD31$^+$Sca-1$^+$CD45$^-$Ter119$^-$ endothelial cells (ECs), and CXCL12-GFP$^-$CD31$^-$Sca-1$^-$CD45$^-$Ter119$^-$ cells from the bone marrow fraction and CXCL12-GFP^{lo}OPN$^-$, CXCL12-GFP^{lo}OPN$^+$, and CXCL12-GFP$^-$OPN$^+$ cells from the bone fraction of CXCL12-GFP mice. Results are expressed as fold difference compared to the levels found in CAR cell samples (G3PDH normalization). n = 4.

(B) The amount of SCF and CXCL12 protein per single femur from wild-type and CXCL12-DTR-GFP mice at 3 days after DT administration by enzyme-linked immunosorbent assay (ELISA). n = 3; *p < 0.05.

(C–E) CD34$^-$Lin$^-$Sca-1$^+$c-kit$^+$CD150$^+$CD48$^-$ HSCs from wild-type mice were sorted and cultured. (C) QRT-PCR analysis of mRNA expression of Cyclin D1, D2, A2, Cdc6, Mad1, and Evi-1 in HSCs before and after 6 hr culture in serum alone or with SCF. n = 3; *p < 0.05. (D) Flow-cytometric analysis of cell size of HSCs cultured in serum alone (green line) or with SCF (orange line) for 12 hr by FSC. (E) QRT-PCR analysis of mRNA expression of Cyclin D1 and Mad1 in HSCs before and after 6 hr culture in serum alone or with CXCL12. n = 3; *p < 0.05. Results are expressed as fold difference compared to the levels found in freshly isolated HSCs (G3PDH normalization) (C and E).

All error bars represent SD of the mean (A–C and E).

CXCL12-GFP$^-$CD31$^-$Sca-1$^-$CD45$^-$Ter119$^-$ cells from the bone marrow fraction, and CXCL12-GFP^{lo}OPN$^-$, CXCL12-GFP^{lo}OPN$^+$, and CXCL12-GFP$^-$OPN$^+$ cells from the bone fraction of CXCL12-GFP mice revealed that the expression of SCF and CXCL12 was considerably higher in CAR cells than in other populations examined (Figure 5A). Consistent with this, the protein expression of SCF and CXCL12 was severely reduced in the bone marrow from CAR cell-depleted mice, supporting the idea that CAR cells are the major producer of SCF and CXCL12 in the marrow (Figure 5B). Single-cell RT-PCR analysis revealed that all individual cells (52 of 52; 100%) within the CAR cell population expressed SCF in the bone marrow from CXCL12-GFP mice, suggesting that individual CAR cells express high amounts of SCF as well as CXCL12. These results are in line with the facts that SCF augments the proliferation of B cell and erythroid progenitors in culture (Martin et al., 1990), that administration of a selective inhibitor (imatinib) of c-kit, c-abl, and platelet-derived growth factor receptor (PDGFR) tyrosine kinases led to a reduction in the numbers of CLPs, pro-B cells, MEPs, and proerythroblasts and to a modest reduction in the cell size of HSCs (Figure S5), and that the numbers of CLPs, pro-B cells, and proerythroblasts are severely reduced in mice lacking SCF receptor c-kit or CAR cells.

Like HSCs from CAR cell-depleted mice, wild-type HSCs cultured in serum alone revealed altered expression of genes involved in cell-cycle promotion, DNA replication, and early myeloid differentiation and had a decreased cell size, as described above (Figures 4B–4D). SCF completely rescued the mRNA expression of Cyclin D1, D2, Cdc6, and Mad1 in HSCs (Figure 5C) and the cell size of HSCs (Figure 5D) in the culture for 6 hr. In contrast, SCF did not rescue the expression of Cyclin A2 and downregulated the expression of Evi-1 during SCF treatment (Figure 5C). In contrast, CXCL12 partially rescued the expression of Cyclin D1 and Mad1 (Figure 5E). These results suggest that SCF and CXCL12 partially contribute to the niche functions of CAR cells in HSC maintenance.

Individual CAR Cells Express both Adipogenic and Osteogenic Genes

We sought to identify the lineage nature of CAR cells. Flow-cytometric analysis of bone marrow from CXCL12-GFP mice revealed that CXCL12-GFP^{hi} CAR cells exhibited a largely homogeneous expression of cell-surface proteins, including VCAM-1, CD44, CD51 (αv integrin), PDGFRα and PDGFRβ, suggesting that CAR cells consist of a relatively homogeneous population (Figure S6A). We analyzed mRNA expression of lineage-specific markers in sorted non-hematopoietic cell populations from the bone marrow and bone fractions of CXCL12-GFP mice. QRT-PCR analysis has shown that the expressions of C/EBPα and peroxisome proliferator-activated receptor γ (PPARγ), which are essential for adipocyte differentiation (Barak et al., 1999), and Runx2 and Osterix, which are essential for osteogenic progenitors (Komori et al., 1997; Nakashima et al., 2002), were considerably higher in CAR cells than in other populations

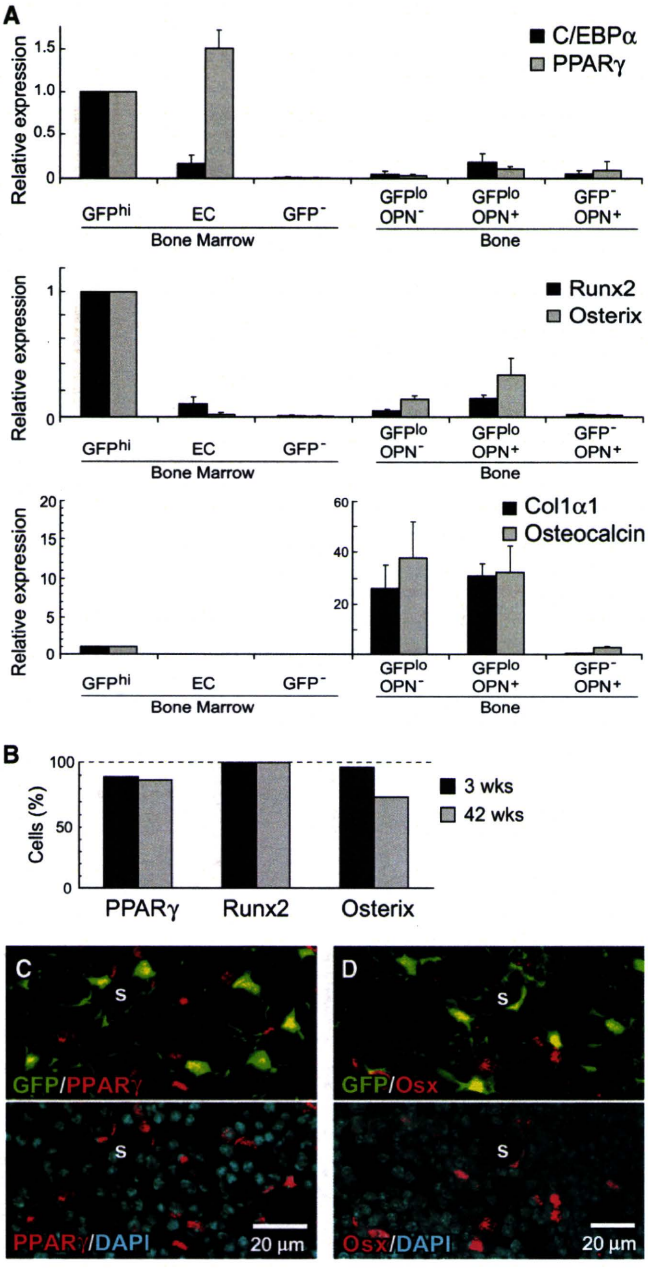

Figure 6. Expression of Requisite Factors for Adipogenesis and Osteogenesis in CAR Cells

(A) QRT-PCR analysis of sorted CXCL12-GFP^{hi}CD45$^-$Ter119$^-$ CAR cells, CD31$^+$Sca-1$^+$CD45$^-$Ter119$^-$ endothelial cells (ECs), and CXCL12-GFP$^-$ CD31$^-$Sca-1$^-$CD45$^-$Ter119$^-$ cells from the bone marrow fraction and CXCL12-GFP^{lo}OPN$^-$, CXCL12-GFP^{lo}OPN$^+$, and CXCL12-GFP$^-$OPN$^+$ cells from the bone fraction of CXCL12-GFP mice. mRNA levels of C/EBPα, PPARγ, Runx2, Osterix, Col1α1, and Osteocalcin. CAR cell samples have been normalized to 1. Error bars represent SD of the mean; n = 4.

(B) Single-cell RT-PCR analysis of the frequency of cells expressing PPARγ, Runx2, and Osterix in sorted CAR cells. n = 2.

(C) Bone marrow sections from 14-week-old CXCL12-GFP mice stained with antibodies against PPARγ (red). Most CAR cells (green) express PPARγ (yellow).

(D) Bone marrow sections from 3-week-old growing CXCL12-GFP mice stained with antibodies against Osterix (red). Most CAR cells (green) express Osterix (yellow). In (C) and (D), the nuclei of cells were labeled with DAPI dye (blue); S, vascular sinus.

examined (Figure 6A). The expression of type I collagen and osteocalcin, which are abundant in osteoblasts, was much lower in CAR cells than in CXCL12-GFP^{lo}OPN$^+$ or CXCL12-GFP^{lo} OPN$^-$ cells from the bone fraction (Figure 6A). Furthermore, we observed a higher expression of BMPRIA and PPR, which regulate bone formation and HSC niche function (Calvi et al., 2003; Zhang et al., 2003), in CAR cells than in other cell populations (Figure S6B). To address the possibility that distinct adipogenic and osteogenic progenitors are included in the CAR cell population, we analyzed the expression of adipogenic and osteogenic genes in CAR cells at the single-cell level. Single-cell RT-PCR analysis revealed that most or all individual cells within the CAR cell population expressed PPARγ, Runx2, and Osterix in bone marrow from CXCL12-GFP mice, suggesting that most CAR cells are adipo-osteogenic bipotential progenitors (Figure 6B). Consistent with this, immunohistochemical analysis of bone marrow revealed that most CAR cells expressed PPARγ protein (Figure 6C). In addition, Osterix protein expression was observed in many CAR cells as well as bone-lining osteoblasts in 3-week-old growing CXCL12-GFP mice (Figure 6D and data not shown).

Individual CAR Cells Have Potential to Differentiate into Adipocytic and Osteoblastic Cells

We analyzed the ability of CAR cells to differentiate into adipocytic and osteoblastic cells in vitro. When CAR cells were sorted, most of these cells died immediately in culture. Thus, we cultured whole bone marrow cells from CXCL12-GFP mice in medium containing a PPARγ activator, pioglitazone. In the cultures, most CXCL12-GFP$^+$ CAR cells appeared to remain viable and many CAR cells (63%) differentiated into multivacuolar lipid-containing preadipocytes, as assessed by Nile Red staining (Figures 7A and 7B), suggesting that the majority of CAR cells have the potential to differentiate into adipocytic cells in vitro. Subsequently, we cultured whole bone marrow cells from CXCL12-GFP mice in the presence of BMP-2 and analyzed the expression of an osteoblast differentiation-related marker, ALP, in individual CAR cells. In the cultures, most CAR cells appeared to remain viable, and the majority of CAR cells (90%) exhibited high ALP activity (Figure 7C and Figure S7). Because histological analysis of bone marrow has shown that only bone-lining mature osteoblasts exhibited high ALP activity (Figure 1C), these results suggest that most CAR cells have potential to differentiate into mature osteoblasts.

Next, we analyzed the ability of CAR cells to differentiate into adipocytic cells in vivo. It has been shown previously that multivacuolar lipid-containing precursors of adipocytes appear in the bone marrow of humans and mice in the early aplastic phase following chemotherapy (Bianco et al., 1988). We injected CXCL12-GFP mice with 250 mg/kg of 5-fluorouracil (5-FU), which preferentially eliminates proliferating cells. Multivacuolar lipid-containing CAR cells, as assessed by Nile Red staining, were observed in the bone marrow 7 days after 5-FU injection (Figure 7D). Some of these multivacuolar lipid-containing CAR cells surrounded sinusoidal endothelial cells, and others did